

## Nanoparticle Charge and Size Control Foliar Delivery Efficiency to Plant Cells and Organelles

Peiguang Hu, Jing An, Maquela Matamis Faulkner, Honghong Wu, Zhaohu Li, Xiaoli Tian, and Juan Pablo Giraldo

ACS Nano, Just Accepted Manuscript • DOI: 10.1021/acsnano.9b09178 • Publication Date (Web): 06 Jul 2020

Downloaded from pubs.acs.org on July 6, 2020

### Just Accepted

“Just Accepted” manuscripts have been peer-reviewed and accepted for publication. They are posted online prior to technical editing, formatting for publication and author proofing. The American Chemical Society provides “Just Accepted” as a service to the research community to expedite the dissemination of scientific material as soon as possible after acceptance. “Just Accepted” manuscripts appear in full in PDF format accompanied by an HTML abstract. “Just Accepted” manuscripts have been fully peer reviewed, but should not be considered the official version of record. They are citable by the Digital Object Identifier (DOI®). “Just Accepted” is an optional service offered to authors. Therefore, the “Just Accepted” Web site may not include all articles that will be published in the journal. After a manuscript is technically edited and formatted, it will be removed from the “Just Accepted” Web site and published as an ASAP article. Note that technical editing may introduce minor changes to the manuscript text and/or graphics which could affect content, and all legal disclaimers and ethical guidelines that apply to the journal pertain. ACS cannot be held responsible for errors or consequences arising from the use of information contained in these “Just Accepted” manuscripts.

# Nanoparticle Charge and Size Control Foliar Delivery Efficiency to Plant Cells and Organelles

Peiguang Hu<sup>1,‡</sup>, Jing An<sup>2,1,‡</sup>, Maquela M. Faulkner<sup>1</sup>, Honghong Wu<sup>1,†</sup>, Zhaohu Li<sup>2</sup>, Xiaoli Tian<sup>2</sup>,  
Juan Pablo Giraldo<sup>1\*</sup>

<sup>1</sup>Department of Botany and Plant Sciences, University of California, Riverside, California  
92521, USA

<sup>2</sup>State Key Laboratory of Plant Physiology and Biochemistry, College of Agronomy and  
Biotechnology, China Agricultural University, Beijing 100193, China

<sup>‡</sup>These authors contributed equally.

\*Corresponding Author: [juanpablo.giraldo@ucr.edu](mailto:juanpablo.giraldo@ucr.edu)

## Abstract

Fundamental and quantitative understanding of the interactions between nanoparticles and plant leaves is crucial for advancing the field of nano-enabled agriculture. Herein, we systematically investigated and modeled how zeta potential (-52.3 mV to +36.6 mV) and hydrodynamic size (1.7-18 nm) of hydrophilic nanoparticles influence delivery efficiency and pathways to specific leaf cells and organelles. We studied interactions of nanoparticles of agricultural interest including carbon dots (CDs, 0.5 and 5 mg/mL), cerium oxide (CeO<sub>2</sub>, 0.5 mg/mL) and silica (SiO<sub>2</sub>, 0.5 mg/mL) nanoparticles with leaves of two major crop species having contrasting leaf anatomies: cotton (dicotyledon) and maize (monocotyledon). Biocompatible CDs allowed real-time tracking of nanoparticle translocation and distribution *in planta* by confocal fluorescence microscopy at high spatial (~200 nm) and temporal (2-5 min) resolution. Nanoparticle formulations with surfactants (Silwet L-77) that reduced surface tension to 22 mN/m were found

1  
2  
3 to be crucial for enabling rapid uptake (< 10 min) of nanoparticles through the leaf stomata and  
4 cuticle pathways. Nanoparticle-leaf interaction (NLI) empirical models based on hydrodynamic  
5 size and zeta potential indicate that hydrophilic nanoparticles with less than 20 and 11 nm for  
6 cotton and maize, respectively, and positive charge (> 15 mV), exhibit the highest foliar delivery  
7 efficiencies into guard cells (100%), extracellular space (90.3%), and chloroplasts (55.8%).  
8 Systematic assessments of nanoparticle-plant interactions would lead to the development of NLI  
9 models that predict the translocation and distribution of nanomaterials in plants based on their  
10 chemical and physical properties.  
11  
12  
13  
14  
15  
16

### 17 18 **Keywords**

19  
20  
21 carbon dots, cerium oxide nanoparticles, silica nanoparticles, surfactant, crops, agriculture.  
22  
23  
24

25 The rapid growth in human population will require about 60% increase or more in food  
26 production by 2050 relative to 2005-2007.<sup>1</sup> However, recent increases in annual crop yield rates  
27 from 2005 to 2014 are significantly lower than those in preceding years<sup>2</sup> and far behind those  
28 required to secure the food demand in 2050.<sup>3-5</sup> Furthermore, climate change is exacerbating the  
29 frequency and intensity of major environmental stresses such as drought, heat, and pathogen  
30 infections that negatively impact crop productivity.<sup>6-8</sup> Agricultural production faces many other  
31 challenges including largely inefficient use of resources such as fertilizers, pesticides, and  
32 herbicides used for improving crop yields. About 40-90% of these agrochemicals are lost to the  
33 environment and never reach their target in plants.<sup>9-11</sup> This unsustainable use of resources leads  
34 to not only massive economic and energy losses but also significant negative environmental  
35 pollution.<sup>12-15</sup> Improvement in crop yields will require convergent and multidisciplinary  
36 approaches for enhancing plant tolerance to environmental and pathogen stresses and the  
37 efficient use of resources.  
38  
39  
40  
41  
42  
43  
44  
45  
46  
47  
48

49 Nanoscale materials exhibit distinct physical and chemical properties that enable them to act as  
50 unique tools for research and development of agricultural technologies.<sup>16-21</sup> Nanomaterials have  
51 been demonstrated to improve plant tolerance to environmental<sup>22-24</sup> and biotic stresses,<sup>25-27</sup> to  
52 enhance agrochemical delivery efficiency,<sup>17,28-32</sup> to act as sensors that monitor plant signaling  
53  
54  
55  
56  
57  
58  
59  
60

1  
2  
3 molecules and pollutants in the environment,<sup>33–37</sup> and to facilitate gene delivery to plant nuclear  
4 and plastid genomes.<sup>38,39</sup> Currently, the main strategies employed for nanomaterial delivery to  
5 plants in the field are soil drenching,<sup>40–44</sup> feeding/injection,<sup>22,24,28,33–35,38,39,45–48</sup> and foliar  
6 delivery.<sup>46–60</sup> Most nanoparticles applied to soil are not taken up by plants due to nanomaterial  
7 heteroaggregation in soil, soil runoff, or root biological barriers.<sup>41,61–65</sup> Although  
8 feeding/injection methods are highly efficient to deliver nanomaterials directly into plants, they  
9 are labor intensive.<sup>22,24,28,33–35,38,39,49</sup> Foliar topical delivery provides an efficient and scalable  
10 approach for directly interfacing nanomaterials with plants. However, a poor understanding of  
11 how nanoparticle chemical and physical properties control the translocation, distribution, and  
12 attachment of nanomaterials in plant leaves limits the use of nanotechnology in nano-enabled  
13 agriculture.  
14  
15  
16  
17  
18  
19  
20  
21  
22  
23

24 Previous studies on nanoparticle uptake in plant protoplasts (lacking cell walls)<sup>66</sup> and isolated  
25 chloroplasts<sup>28</sup> *in vitro* have discovered the role that zeta potential and size play on nanoparticle  
26 translocation across plant plasma membrane and organelle lipid bilayers. These studies report  
27 that positively or negatively charged nanoparticles with zeta potential magnitudes higher than 20  
28 or 30 mV (Smoluchowski approximation) are more likely to be taken up by plant cell or  
29 chloroplast membranes, respectively, whereas more neutral nanomaterials are not able to  
30 penetrate plant lipid bilayers. As the size of the nanoparticle decreases, larger magnitude of zeta  
31 potential is needed for enabling translocation across lipid membranes. However, a systematic and  
32 modeling study of how charge and size influence nanoparticle transport *in vivo* from the leaf  
33 surface (epidermis) into leaf cells and their organelles has not been performed. *In vivo*  
34 nanoparticle translocation across leaves requires them to cross not only cell and organelle lipid  
35 membranes but also the leaf cuticle, stomatal pores, and cell walls (Figure 1a). The leaf surface  
36 is formed by a waxy layer called the cuticle containing nanoscale (~2 nm) hydrophilic pores,<sup>49,67–</sup>  
37 <sup>71</sup> and micron scale stomatal pores. The cuticle and stomata are main pathways for nanomaterial  
38 delivery to plant leaves. Inside leaves, the cell wall is a biological barrier with both hydrophobic  
39 and hydrophilic components,<sup>72</sup> with a reported pore size less than 13 nm,<sup>73</sup> and unequal  
40 distribution of fixed negative charges.<sup>74,75</sup> The upper size exclusion limit for transport of  
41 nanoparticles through plant cells and the impact of charge on nanoparticle translocation across  
42 these cells remains unclear.<sup>75–77</sup>  
43  
44  
45  
46  
47  
48  
49  
50  
51  
52  
53  
54  
55  
56  
57  
58  
59  
60

1  
2  
3  
4  
5 Herein, we systematically investigated and modeled how nanomaterial zeta potential and  
6 hydrodynamic size impact the interactions of hydrophilic nanoparticles with leaf cell surfaces  
7 and organelle membranes of chloroplasts, key plant photosynthetic organelles. We designed and  
8 synthesized ten types of nanoparticles including fluorescent carbon dots (CDs), CeO<sub>2</sub> (NC) and  
9 SiO<sub>2</sub> (SN) nanoparticles (NP) to study how nanoparticle properties affect their translocation  
10 across leaf biological barriers and their distribution in leaf cells. CDs are bright and fluorescent  
11 nanomaterials with high quantum yield, high resistance to photobleaching, tunable emission  
12 range,<sup>78–81</sup> and facile surface functionalization. These biocompatible nanomaterials<sup>82–84</sup> have  
13 been used for improving plant growth and disease resistance, and bioimaging in whole  
14 plants.<sup>60,85,86</sup> The unique optical properties of CDs are optimal for high spatial and temporal  
15 resolution imaging by confocal microscopy<sup>84</sup> and studying nanoparticles interactions with leaf  
16 biological barriers. CeO<sub>2</sub> NPs acting as catalytic antioxidants have been delivered to chloroplasts  
17 in plant model systems to improve plant tolerance to stresses including heat, chilling, high-  
18 light,<sup>24</sup> and salinity.<sup>22</sup> The SiO<sub>2</sub> NPs have been reported to act as gene and agrochemical delivery  
19 platforms,<sup>87–90</sup> and to improve crop yield.<sup>90–92</sup>  
20  
21  
22  
23  
24  
25  
26  
27  
28  
29  
30

31  
32 We tested the overarching hypothesis that nanomaterial zeta potential and size determine the  
33 translocation and distribution of nanoparticles in leaf cells of plants with contrasting leaf  
34 anatomies, cotton (*Gossypium hirsutum* L.) and maize (*Zea mays* L.), corresponding to the major  
35 plant taxa of dicotyledons and monocotyledons, respectively. Only one previous study has  
36 compared nanoparticle interactions between dicotyledons and monocotyledons, reporting  
37 differences in translocation from roots to shoots.<sup>93</sup> To accomplish this study's overarching goal,  
38 1) we synthesized and characterized CDs, CeO<sub>2</sub>, and SiO<sub>2</sub> NPs with specific fluorescent  
39 emission properties, positive or negative zeta potential, and specific hydrodynamic diameters; 2)  
40 we developed nanoparticle formulations containing surfactants and studied the influence of  
41 surface tension on enabling rapid and efficient foliar nanoparticle delivery for potential nano-  
42 enabled agricultural applications; 3) we developed approaches for imaging nanoparticle  
43 translocation in leaves by confocal fluorescence microscopy at high spatial and temporal  
44 resolution; 4) we assessed how nanoparticle zeta potential and hydrodynamic size influence their  
45 distribution in leaf cells and organelles including stomatal guard cells, extracellular space and  
46  
47  
48  
49  
50  
51  
52  
53  
54  
55  
56  
57  
58  
59  
60

1  
2  
3 chloroplasts; and 5) we created nanoparticle-leaf interactions (NLI) empirical models based on  
4 nanomaterial zeta potential and hydrodynamic size for designing nanoparticles with higher  
5 delivery efficiency into specific leaf cellular compartments.  
6  
7  
8  
9

## 10 11 **Results and Discussion**

### 12 13 14 **Characterization of plant leaves with different anatomy**

15  
16 The cuticle and stomata are the two main pathways of nanomaterial entry through the leaf  
17 epidermis into the mesophyll (Figure 1a). Inside leaves, nanomaterials can translocate across  
18 extracellular (apoplastic) and/or intracellular (symplastic) pathways in the mesophyll. To enter  
19 leaf mesophyll cells and chloroplasts from the extracellular space (apoplast), nanoparticles have  
20 to cross main plant biological barriers such as the cell wall, plasma and organelle membranes.  
21 Leaf anatomical differences between maize (monocot) and cotton (dicot) leaves are illustrated in  
22 scanning electron microscopy (SEM) images of the leaf surface (Figure 1b), and light  
23 microscopy images of leaf cross-sections (Figure 1c). The density of dumbbell shaped stomata in  
24 the leaf epidermis of maize,  $34.3 \pm 4.6 \text{ mm}^{-2}$ , is eight times lower than that of kidney shaped  
25 stomata in cotton leaves,  $258.4 \pm 32.2 \text{ mm}^{-2}$  ( $P < 0.01$ , Figure S1a). In contrast, the stomatal  
26 length in maize leaves,  $34.3 \pm 0.4 \text{ }\mu\text{m}$ , is more than twice higher than that of cotton leaves,  $13.4$   
27  $\pm 0.8 \text{ }\mu\text{m}$  ( $P < 0.001$ , Figure S1b). Both palisade and spongy mesophyll cells can be identified in  
28 the leaf mesophyll of cotton leaves, whereas only one type of mesophyll cells characteristic of  
29 maize leaves can be observed. In the cotton leaf, the palisade mesophyll cells are closely packed  
30 side-by-side below the adaxial (upper) leaf side, leaving little extracellular air space in between  
31 them except underneath the stomatal pores. The spongy mesophyll cells in cotton leaves are  
32 sparsely distributed on the abaxial (lower) leaf side creating large extracellular air spaces. In  
33 contrast, tightly packed mesophyll cells were observed in the maize leaf cross-section, leaving  
34 small air spaces underneath the stomatal pores. These leaf anatomical traits for cotton and maize  
35 are characteristic of dicotyledonous and monocotyledonous plant species, respectively.<sup>94</sup> Leaf  
36 autofluorescence spectra for crop leaves were independent of the excitation wavelength (405,  
37 476, and 514 nm) used for confocal microscopy imaging (Figure S2). However, variations in  
38  
39  
40  
41  
42  
43  
44  
45  
46  
47  
48  
49  
50  
51  
52  
53  
54  
55  
56  
57  
58  
59  
60

1  
2  
3 chlorophyll a/b ratios in cotton and maize leaves can result in slight differences in pigment  
4 autofluorescence spectra between these plant species<sup>95,96</sup> (Figure 2c and S2).  
5  
6  
7

### 8 **Nanoparticle chemical and physical properties**

9  
10 Hydrodynamic size measurements by DLS (dynamic light scattering) confirmed the synthesis of  
11 CDs, CeO<sub>2</sub>, and SiO<sub>2</sub> nanoparticles with average size from 1.7 to 18.0 nm (Table S1, average ±  
12 standard deviation) (Figure 2a). Representative TEM images show the core size of nanoparticles  
13 in similar range from 1 to 15 nm (Figure S3). Nanoparticle zeta potentials from -52.3 mV to  
14 +36.6 mV (Table S1, average ± standard deviation) were significantly different except between  
15 SA-CD6 and DiI-PNC11, DiI-PNC2 and FITC-SN18 ( $P < 0.05$ ) (Figure 2b). Zeta potential of  
16 PEI-CDs (polyethyleneimine coated CDs), and DiI-ADNCs (DiI labeled aminated dextran  
17 coated NC) are positive due to surface functionalization with amine-rich coatings. In contrast,  
18 SA-CDs (succinic anhydride modified PEI-CDs), DiI-PNCs, [DiI labeled poly (acrylic acid)  
19 coated NCs], and FITC-SN18 (FITC labeled SN) exhibit negative zeta potentials because of  
20 abundant carboxyl or silanol groups on the surface. The surface chemical composition of  
21 nanoparticles was confirmed by Fourier-transform infrared spectroscopy (FTIR) showing the  
22 successful functionalization of the nanomaterial surface by different coatings (Figure S4). We  
23 designed the nanoparticles for high resolution confocal microscopy imaging by minimizing their  
24 fluorescence emission overlap with leaf autofluorescence (Figure 2c and S2). The nanoparticle  
25 excitation wavelengths in both confocal microscopy and *in vitro* fluorescence measurements  
26 were set at 405, 514, and 476 nm for CDs, DiI-NCs and FITC-SN18, respectively, close to the  
27 absorption maximum in UV-vis absorption spectra (Figure S5). Nanoparticle fluorescence  
28 emission ranges from 410 to 600 nm for CDs, 550 to 650 nm for DiI-NCs, and 500 to 600 nm for  
29 FITC-SN18, with no significant overlap with the leaf autofluorescence from 670 to 800 nm  
30 (Figure 2c and S2).  
31  
32  
33  
34  
35  
36  
37  
38  
39  
40  
41  
42  
43  
44  
45  
46

### 47 **Influence of formulation surface tension on nanoparticle foliar delivery**

48 Surfactants are widely used in agrochemical formulations for improving contact with plant  
49 surfaces.<sup>97-102</sup> To the best of our knowledge there are no studies assessing their role and impact  
50 on nanoparticle foliar delivery efficiency. The leaf surface of cotton and maize plants was  
51 interfaced with CDs of different size and charge that were previously suspended in nanoparticle  
52  
53  
54  
55  
56  
57  
58  
59  
60

1  
2  
3 formulations with surface tension about 30 mN/m or 22 mN/m by adding Triton X-100 or Silwet  
4 L-77, respectively. Nanoparticles did not affect the formulation surface tension and maintained  
5 formulation pH values (5.3 - 8.5) within the plant physiological range (pH 5-8) (Figure S6). Leaf  
6 uptake was determined as fluorescence of CDs observed in the leaf extracellular space,  
7 mesophyll cells, or both. Confocal fluorescence microscopy images of leaves exposed to CDs  
8 (after 3 h) (Figure 3 and S7) indicated that formulations containing Silwet L-77 with relatively  
9 low surface tension allowed CDs of 2-6 nm size to penetrate through the leaf surface. In contrast,  
10 formulations with Triton X-100 having a higher surface tension only allowed CDs of 2 nm size  
11 to enter maize leaves (Figure 3 and S7). Therefore, we assessed nanoparticle foliar translocation  
12 and distribution using Silwet L-77, the more effective surfactant. Non-surfactant-containing  
13 formulations had poor wettability on the leaf surface, forming semi-spherical or spherical drops  
14 on cotton and maize leaf surfaces. Confocal microscopy images taken from leaf tissues right  
15 underneath the area of nanoparticle exposure indicated that no CDs suspended in water without  
16 surfactant translocated inside leaves (Figure S8). Similarly, Avellan *et al.* applied gold  
17 nanoparticles in aqueous solution without surfactant on wheat leaves and reported significantly  
18 reduced amounts (~20%) of hydrophilic gold nanoparticle (3 nm, zeta potential -69.2 mV,  
19 concentration 10 mg-Au/L) adhesion to wheat leaves (2 h after exposure), compared to 100% for  
20 amphiphilic gold nanoparticles (3 nm, zeta potential -56.8 mV, concentration 10 mg-Au/L).<sup>103</sup>  
21  
22  
23  
24  
25  
26  
27  
28  
29  
30  
31  
32  
33  
34  
35

36 These results were further confirmed with 3D images created from confocal microscopy z-stack  
37 images (2  $\mu\text{m}$  z-axis resolution and 225-285 nm x-y resolution, Leica SP5) of cotton and maize  
38 leaves treated with 10 different types of fluorescent nanoparticles in formulations with Silwet L-  
39 77 (Figure S9). Nanoparticles in surfactant formulations exhibited high stability (Figure S10).  
40 Fluorescent dye molecules strongly associated with the cerium oxide and silica nanoparticles and  
41 no dissociation occurred even in the presence of Silwet L-77 (Figure S11). In cotton, all the  
42 nanoparticles with hydrodynamic size up to 18 nm penetrated the leaf surface (Figure S9a). In  
43 contrast, nanoparticles with hydrodynamic size larger than 8 nm were not permeable through the  
44 maize leaf surface (Figure S9b). The surfactant concentrations used in this study were similar to  
45 those used in actual agricultural formulations<sup>98,99</sup> and do not have a detrimental impact on leaf  
46 health in cotton and maize (Figure S12). The CD formulations in Silwet L-77 as surfactant were  
47 designed to be biocompatible with plants by monitoring the impact of formulation exposure on  
48  
49  
50  
51  
52  
53  
54  
55  
56  
57  
58  
59  
60



1  
2  
3 leaf chlorophyll content. No significant differences of leaf chlorophyll content were observed  
4 between control untreated leaves and those interfaced with CDs suspended in formulations with  
5 Silwet L-77 (Figure S12). Chlorophyll content indexes measured with a SPAD meter before and  
6  
7 3h after exposure of leaves to nanoparticles were similar (Figure S12) indicating that  
8  
9 nanoparticle exposure does not interfere with SPAD meter readings.  
10  
11  
12

### 13 **High spatial and temporal resolution imaging of nanoparticle translocation in leaves *in*** 14 ***planta*** 15

16  
17 Leaves of intact plants mounted on a confocal microscope were treated with positively or  
18 negatively charged CDs, PEI-CD2, PEI-CD6, SA-CD2, and SA-CD6 with hydrodynamic sizes  
19 of 2 and 6 nm, previously suspended in formulations with Silwet L-77. Z-stack images were  
20 collected every 2 to 5 min from the leaf surface to the mesophyll (2  $\mu\text{m}$  z-axis resolution and 206  
21 - 233 nm x-y resolution, Zeiss 880), generating time-lapse videos of nanoparticle pathways of  
22 translocation across leaves in real-time and *in planta* (Video S1, S2, S5, S6, S9, S10, S13, and  
23 S14). Snapshots of our real-time confocal microscopy videos within the leaf epidermis and  
24 mesophyll layers, and the reconstructed 3D images from z-stacks suggest different pathways of  
25 foliar entrance for PEI-CD2, SA-CD2, PEI-CD6, and SA-CD6 in cotton and maize leaves  
26 (Figure 4 and S13-S15, Video S3, S4, S7, S8, S11, S12, S15, and S16). All CDs translocated  
27 across the cotton leaf surface through both stomatal and cuticular pathways (Figure 4 and S13-  
28 S15, Video S1, S3, S5, S7, S9, S11, S13, and S15). In contrast, stomata were the main pathway  
29 of entrance for all the four CDs in maize leaves, highlighting potential differences of  
30 nanoparticle translocation between monocots (maize) and dicots (cotton) (Figure 4 and S13-S15,  
31 Video S2, S4, S6, S8, S10, S12, S14, and S16). The presence of nanoparticle fluorescence  
32 signals in stomatal guard cells or pores in both plant species indicates translocation through the  
33 stomatal pathway (Figures 4 and S13-S15). Species dependent differences in initial nanoparticle  
34 translocation through either stomatal pores (Figure 4, maize), guard cells or both (Figure 4,  
35 cotton) are interesting subjects of future studies on translocation of nanoparticles within stomatal  
36 structures. Nanoparticle fluorescence is also observed around the epidermal cell boundaries in  
37 cotton and to a much less extent in maize (Figures 4, S13-S15) suggesting that nanoparticles are  
38 distributed within anticlinal cell walls rich in hydrophilic pores.<sup>73</sup> The hydrophilic pores in the  
39  
40  
41  
42  
43  
44  
45  
46  
47  
48  
49  
50  
51  
52  
53  
54  
55  
56  
57  
58  
59  
60

1  
2  
3 cuticle have been reported to be smaller than 2 nm<sup>67–69</sup> representing a likely size exclusion limit  
4 factor for larger hydrophilic nanoparticles.  
5  
6  
7

8 For both cotton and maize plants, the CDs rapidly entered the leaves within only a few minutes  
9 after nanoparticle exposure and localized within different cellular intracellular and extracellular  
10 compartments in the leaf mesophyll within 1 hr. Nanomaterials can rapidly penetrate plant cell  
11 membranes *via* non-endocytic pathways<sup>24,104</sup> by disrupting lipid bilayers.<sup>28,66</sup> Previous studies  
12 have reported transport of nanoparticles across the leaf surface but in significantly longer time  
13 frames of several hours or days after nanoparticle exposure.<sup>71,103</sup> Avellan *et al.* recently reported  
14 using X-ray mapping that hydrophilic citrate-Au NPs, especially those about 3 nm in size, are  
15 preferentially taken through the stomatal pathway in wheat (monocot).<sup>103</sup> Surface chemistry also  
16 influences gold nanoparticle (AuNPs) translocation through the leaf surface.<sup>103</sup> Coating Au NPs  
17 with polyvinylpyrrolidone (PVP, an amphiphilic polymer) led to complete uptake through the  
18 leaf, while the hydrophilic citrate coating left a large fraction of Au NPs on the leaf surface.<sup>103</sup>  
19  
20  
21  
22  
23  
24  
25  
26  
27  
28

### 29 **Impact of nanoparticle charge and size on their distribution in leaf cells and organelles**

30 We assessed by confocal fluorescence microscopy how hydrodynamic size and zeta potential of  
31 CD, CeO<sub>2</sub> and SiO<sub>2</sub> NPs affect their distribution in leaf cells and organelles including guard  
32 cells, extracellular space, and chloroplasts (Figure 5 and S16-S19). Guard cells are important  
33 cellular structures regulating CO<sub>2</sub> and H<sub>2</sub>O gas exchange,<sup>105,106</sup> and the gates for plant pathogen  
34 infections.<sup>107</sup> The extracellular space exhibits marked differences between cotton and maize  
35 (Figure 1) and is characterized by a low pH (~5)<sup>108</sup> that could significantly influence  
36 transformations of nanoparticles for agrochemical delivery. Translocation of nanoparticles into  
37 cells and photosynthetic organelles such as chloroplasts requires movement across major plant  
38 cellular barriers such as the cell wall, plasma membrane and organelle lipid bilayers. The  
39 colocalization rate of nanoparticles with chloroplasts (Figure 5b) was analyzed by identifying  
40 overlapped fluorescence peaks in six transects of ROI (region of interest) equidistantly separated  
41 in confocal image overlays (See methods) as described in previous studies.<sup>24,109</sup> The chloroplast  
42 colocalization rate with nanoparticles assessed by ROI analysis was confirmed by Manders'  
43 overlap coefficient analysis<sup>110</sup> based on the percentage of chloroplast pixels overlapping with  
44 nanoparticle pixels. The colocalization rates based on ROI analysis and Manders' overlap  
45  
46  
47  
48  
49  
50  
51  
52  
53  
54  
55  
56  
57  
58  
59  
60

1  
2  
3 coefficients were positively correlated ( $P < 0.0001$ ) (Figure S20). Nanoparticles were localized  
4 in the extracellular space of the leaf mesophyll (Figure 5c) as the nanoparticle occupied area  
5 outside the cell boundary delineated by chloroplasts in confocal microscopy imaging (Figure  
6 S21).<sup>111–113</sup> Nanoparticles were identified in guard cells by performing z-stacks as described  
7 above from the stomata upper surface in the leaf epidermis into the leaf mesophyll (Figure 5d).  
8 As shown in the orthogonal views of confocal microscopy images (Figure 5d, after 3 h  
9 exposure), the nanoparticle fluorescence is observed within guard cells and also in stomatal  
10 pores.  
11  
12  
13  
14  
15  
16  
17

18  
19 The impact of charge and size on nanoparticle leaf cellular distribution was quantitatively  
20 assessed as the percentage of guard cells, extracellular space area, or chloroplasts containing  
21 nanoparticles (Figure 6). We identified nanoparticles with efficient delivery to guard cells,  
22 extracellular space, or chloroplasts as those with colocalization rates above the average rates  
23 minus SE (standard error) of all nanoparticles tested (Figure 6, see methods). Most nanoparticles  
24 with hydrodynamic size up to 16 and 8 nm, in cotton and maize, respectively, exhibited above  
25 average colocalization with leaf guard cells, and nanoparticles with larger hydrodynamic size  
26 showed significantly lower delivery efficiencies ( $P < 0.05$ ) (Figure 6a). This indicates a  
27 limitation of nanoparticle penetration into guard cells due to the cell wall size exclusion limit that  
28 is likely plant species specific. Patterns of nanoparticle localization in the extracellular space  
29 were complex and varied depending on plant species, charge and size (Figure 6b). In cotton, all  
30 positively charged nanoparticles with a size up to 12 nm were found efficiently localized in the  
31 extracellular spaces but most negatively charged nanoparticles were found at significantly lower  
32 levels in this compartment ( $P < 0.05$ ). In contrast, nanoparticles were efficiently delivered to  
33 extracellular space in maize when the hydrodynamic size was 6–8 nm for positively charged  
34 nanoparticles and 2–6 nm for most negatively charged nanoparticles. Nanoparticles with  
35 hydrodynamic size smaller than 12 and 6 nm for cotton and maize, respectively, tend to have  
36 above average delivery efficiency to chloroplasts in leaf mesophyll cells ( $P < 0.05$ ). In both crop  
37 species, the percentage of chloroplasts colocalized with nanoparticles was higher in nanoparticles  
38 with positive zeta potential compared to their negatively charged counterparts ( $P < 0.05$ ) (Figure  
39 6c). Although colocalization rates with chloroplasts in maize mesophyll cells were above  
40 average for positively charged nanoparticles under 6 nm in size ( $P < 0.05$ ), the colocalization  
41  
42  
43  
44  
45  
46  
47  
48  
49  
50  
51  
52  
53  
54  
55  
56  
57  
58  
59  
60

1  
2  
3 values with chloroplasts were low and did not surpass 30%. The plant cell wall is negatively  
4 charged<sup>74</sup> which can have a higher affinity with positively charged nanoparticles and act as a  
5 cation exchange membrane facilitating their passive translocation across cell walls.<sup>75–77</sup>  
6

7  
8 Moreover, it has been reported that cationic nanoparticles exhibit higher cellular uptake because  
9 of the negative transmembrane electrical potential with respect to the exterior of the cell.<sup>114,115</sup>  
10

11 The topical foliar delivery of nanoparticles suspended in surfactants and without external  
12 mechanical aid used in this study may also play a role in promoting the delivery of positively  
13 charged nanoparticles across cell wall and membranes. We have previously observed and  
14 reported a higher delivery efficiency of negatively charged CeO<sub>2</sub> NPs to *Arabidopsis*  
15 chloroplasts by needleless syringe infusion through the leaf lamina.<sup>24</sup> Overall these results  
16 indicate that nanoparticle delivery efficiency to leaf cells and organelles are influenced by zeta  
17 potential and limited by the cell wall pore size in a plant species dependent way.  
18  
19  
20  
21  
22  
23  
24

25 Leaf anatomical differences in cotton and maize leaves could explain differences in nanoparticle  
26 foliar delivery efficiency. The smaller extracellular air spaces and tightly packed mesophyll cells  
27 in maize leaves contribute to reduce the cell surface area exposed to nanoparticles entering  
28 through stomatal pathways (Figure 1). Higher stomatal density in cotton than in maize leaves  
29 (Figure S1a) provides more micron-sized stomatal pore entrance pathways for nanomaterials.  
30 Furthermore, stomatal guard cells in the epidermis appear to be more permeable and have a  
31 higher nanoparticle size limit than mesophyll cells containing chloroplasts (Figure 6a,c). Stomata  
32 guard cells have cell walls with mechanical properties that allow them to significantly enlarge or  
33 contract<sup>94,116</sup> and have an estimated pore size greater than 20 nm.<sup>69</sup> In contrast, leaf mesophyll  
34 cells do not undergo large changes in volume<sup>94,116</sup> and have smaller cell wall pore size<sup>73</sup>. These  
35 underlying structural and functional properties of plant cell walls may explain the high  
36 colocalization rates with nanoparticles in leaf guard cells (Figure 6). Together these leaf  
37 structural traits contribute to the differences in translocation of nanoparticles into leaf mesophyll  
38 cells and organelles and overall foliar delivery efficiencies.  
39  
40  
41  
42  
43  
44  
45  
46  
47  
48  
49  
50

### 51 **Nanoparticle-leaf interaction models for designing nanoparticle charge and size**

52 We built nanoparticle-leaf interaction (NLI) empirical models to identify and predict  
53 nanoparticle hydrodynamic size and zeta potential ranges that enable nanoparticle foliar topical  
54  
55  
56  
57  
58  
59  
60

1  
2  
3 delivery with above average efficiencies into cotton and maize guard cells, extracellular space,  
4 and chloroplasts (Figure 6d and Table S2). NLI empirical models based on 95% confidence  
5 ellipse regions predict a 20 and 11 nm hydrodynamic size limit for efficient hydrophilic  
6 nanoparticle delivery into cotton and maize guard cells, respectively. These empirical models  
7 also highlight that nanoparticles with positive zeta potential and below this size limit can be  
8 efficiently delivered into chloroplasts and extracellular spaces of cotton leaves. Despite that  
9 FITC-SN18 nanoparticles have a below average delivery efficiency to guard cells in cotton  
10 (~35%), their nanoparticle size and charge overlapped with the 95% confidence ellipse region for  
11 efficient delivery. FITC-SN18 have silanol instead of carboxyl functional groups suggesting that  
12 nanoparticle surface chemical identity is an important factor that should be taken into account by  
13 NLI empirical models.  
14  
15  
16  
17  
18  
19  
20  
21  
22  
23

24 The hydrodynamic size limitation for hydrophilic nanoparticle delivery efficiency indicates that  
25 the plant cell wall pore size is an important barrier for nanoparticle translocation in plants,  
26 excluding hydrophilic nanoparticles depending on their size. Nanoparticles with amphiphilic  
27 coatings such as PVP have been reported to enable the delivery of nanomaterials (~50 nm)<sup>103</sup>  
28 larger than the size exclusion limits found in this study, highlighting the need of *n*-dimensional  
29 NLI models that include not only nanoparticle size and zeta potential, but also hydrophobicity,  
30 aspect ratio, core and surface chemistry. The PVP coated AuNPs penetrate through the  
31 hydrophobic cuticular domains of the leaf epidermis within 2 days. However, these AuNPs had a  
32 lower translocation efficiency through the leaf mesophyll, possibly due to the amphiphilic nature  
33 of PVP surface coating. Under the nanomaterial hydrodynamic size limit, positive charge is  
34 crucial for nanoparticles to have a high delivery efficiency into leaf cells and organelles. The  
35 different behavior between nanoparticles with positive and negative charge could be associated  
36 with the negatively charged cell walls in plants that act as ion exchange surfaces promoting the  
37 penetration of cationic nanoparticles but impeding the anionic ones.<sup>75-77,117,118</sup> High zeta potential  
38 of nanoparticles, independent of charge, has been reported to favor penetration through plant  
39 membranes according to studies and models based on isolated protoplasts and chloroplasts in  
40 which the plant cell wall is absent.<sup>28,66</sup> However, in leaf cotton cells the nanoparticles with the  
41 lowest zeta potential magnitude and hydrodynamic diameter (SA-CD2, -13.8 mV, 2 nm) were  
42 more efficiently delivered to chloroplasts than the other negatively charged nanoparticles. This  
43  
44  
45  
46  
47  
48  
49  
50  
51  
52  
53  
54  
55  
56  
57  
58  
59  
60

1  
2  
3 supports the idea that the size limiting effect of cell walls could be predominant *in vivo*, allowing  
4 the uptake of nanoparticles with smaller size. Understanding the physical and chemical  
5 interactions of nanoparticles with model and isolated cell walls may contribute to elucidate the  
6 underlying mechanisms of these chemical interactions.  
7  
8  
9

## 10 11 **Conclusions**

12  
13  
14  
15 We designed and synthesized nanoparticles, and developed high spatiotemporal resolution  
16 imaging tools for systematically assessing and modeling the role of charge and size on  
17 nanomaterial distribution in leaf cells. We studied rapid foliar delivery methods for nanoparticles  
18 in cotton and maize crops that could be translated to other plant species and field applications.  
19 We demonstrated that it is crucial to lower nanoparticle formulation surface tension ( $\sim 22$  mN/m)  
20 for rapid foliar delivery of hydrophilic nanoparticles with hydrodynamic size larger than 2 nm.  
21 Real time *in planta* confocal microscopy indicated that nanoparticles translocate across leaf  
22 surfaces through stomata and cuticular pathways. Overall, the efficient delivery of nanoparticles  
23 into guard cells, extracellular space, and chloroplasts is dependent on nanoparticle size and  
24 charge, and plant species. Our systematic assessment of nanoparticle charge and size effect on  
25 their leaf cellular distribution is represented in NLI empirical models acting as predicting tools of  
26 the behavior of similar hydrophilic nanoparticles in cotton and maize leaves. The hydrodynamic  
27 size limit for efficient nanoparticle delivery into leaf cells was determined at 20 and 11 nm for  
28 cotton and maize, respectively, which points out to possible different cell wall pore size for these  
29 two plant species. Positive nanoparticle charge results in higher foliar delivery efficiencies into  
30 chloroplasts, possibly due to their higher affinity with the negatively charged plant cell walls and  
31 negative transmembrane electrical potential of the cell membrane. Although cotton and maize  
32 have contrasting leaf anatomic characteristics of the dicotyledons and monocotyledons,  
33 respectively, we expect that other plant species within these large plant taxa would show  
34 variations in hydrodynamic size and zeta potential range for efficient delivery of nanoparticles to  
35 specific cells and organelles. This study provides a framework of tools and approaches to assess  
36 and model the interactions between nanoparticle properties (hydrodynamic size and zeta  
37 potential) and plant cells and organelles *in vivo*.  
38  
39  
40  
41  
42  
43  
44  
45  
46  
47  
48  
49  
50  
51  
52  
53  
54  
55  
56  
57  
58  
59  
60

1  
2  
3 Understanding and modeling the role of nanoparticle charge, size, hydrophobicity and other  
4 chemical and physical properties on their interactions with leaf surfaces will enable a more  
5 efficient and controlled use of nanoscale agrochemicals. Few studies have addressed how  
6 nanoparticle translocation and distribution in plants is affected by shape and composition of  
7 nanomaterials. However, accumulation and transport of gold nanoparticles in plants has been  
8 reported to depend on their aspect ratio<sup>50</sup> and hydrophobicity.<sup>103</sup> Nanoparticle transformations  
9 including corona formation by proteins, lipids, or carbohydrates in different plant species should  
10 also be assessed to determine the nanoparticle stability, uptake and translocation in plant organs  
11 and cell compartments, as well as their toxicity to plants.<sup>119–122</sup> Both nanomaterial size and  
12 surface properties have been reported to play a key role in determining nanoparticle corona  
13 formation in non-plant biological fluids.<sup>119</sup> This in turn is expected to have an impact on  
14 nanoparticle translocation and distribution in plants. However, the formation of plant  
15 biochemical coronas on nanoparticles is poorly understood and has been addressed by only a  
16 handful of studies.<sup>123,124</sup>  
17  
18  
19  
20  
21  
22  
23  
24  
25  
26  
27  
28

29 Similar to the pharmacokinetics field in biomedical research,<sup>125–130</sup> the emergent research area of  
30 plant nanokinetics aims at modeling nanoparticle uptake dynamics and distribution in plants.  
31 Recent studies in this area are highlighting how nanoparticle properties (*e.g.* size, charge) impact  
32 their translocation and distribution in isolated chloroplasts,<sup>28</sup> protoplasts without cell walls,<sup>66</sup> and  
33 *in vivo* in plants as reported in this study. Comparisons between exposure studies at different  
34 timescales would allow the creation of plant nanokinetic models that merge spatial and temporal  
35 nanoparticle-leaf interaction components for determining and quantifying the dynamic behavior  
36 of nanoparticle uptake, translocation, distribution, and excretion in plant structures. Plant  
37 nanokinetic assessments can lead to effective and safe plant-nanotechnology management,  
38 enhancing the efficacy of nanoparticles on plant health while reducing exposure to humans and  
39 the environment.  
40  
41  
42  
43  
44  
45  
46  
47  
48

## 49 **Methods**

### 50 **Synthesis of nanoparticles**

51  
52  
53  
54  
55  
56  
57  
58  
59  
60

1  
2  
3 The CDs were synthesized by modifying a protocol reported by Khan *et al.*<sup>131</sup> Briefly, 2.40 g (40  
4 mmol) of urea (99.2%, Fisher), 1.92 g (10 mmol) of citric acid (CA, 99.7%, Fisher), and 1.35 mL  
5 of ammonium hydroxide ( $\text{NH}_3 \cdot \text{H}_2\text{O}$ , 30~33%, Aldrich) was dissolved into 2 mL of molecular  
6 water (Corning). The mixture was kept in a 50 mL beaker in an oven at 180 °C for 1h and 20min.  
7  
8 After cooled down to room temperature, the product was dissolved in 300 mL of molecular  
9 water, filtered with filter paper (Whatman, pore size, 11  $\mu\text{m}$ ), and the collected filtrate was  
10 denoted as CDs. To synthesize PEI-CD2 and PEI-CD6, the CDs were functionalized with  
11 PEI600 (branched polyethyleneimine, M.W. 600, 99%, Alfa Aesar) and PEI10k (branched  
12 polyethyleneimine, M.W. ~10k, 99%, Alfa Aesar), respectively. The CDs were suspended in  
13 molecular water to yield 4 mL of solution with a CD concentration of 5 mg/mL and the pH  
14 adjusted to 10 by adding NaOH solution (20 mg/mL). This solution was added slowly while  
15 stirring into a 0.8 mL of PEI600 or PEI10k solution (100 mg/mL). The mixture was kept stirring  
16 for 0.5h before being sealed in Falcon tubes and treated at 85 °C for 16h in the oven. The product  
17 was cooled down to room temperature, condensed and purified with a mixture of molecular  
18 water, ethanol (absolute, Fisher), and chloroform (99%, Fisher) by centrifugation at 4,500 rpm  
19 for 5 times. The resulting PEI-CD solution was collected and blown with air for 30 min to  
20 remove ethanol and chloroform residuals. The PEI-CDs were redissolved in molecular water. To  
21 synthesize SA-CD2 and SA-CD6, PEI-CD2 and PEI-CD6 were further treated with succinic  
22 anhydride (SA, 99%, Alfa Aesar). The PEI-CD2 or PEI-CD6 were diluted with molecular water  
23 to yield 1 mL of solution with a concentration of 5 mg/mL. Then this solution was diluted by  
24 adding 3 mL of DMF (*N,N*-dimethylformamide, >99%, Sigma), followed by adding 1 mL of SA  
25 solution (250 mg/mL) in DMF while stirring. The mixture was kept stirring for 3h before  
26 condensed and purified with a mixture of molecular water, ethanol, and chloroform by  
27 centrifugation at 4,500 rpm for 5 times. The resulting SA-CD solution was collected, and blown  
28 with air for 30 min to remove ethanol and chloroform residuals, and SA-CDs were redissolved in  
29 molecular water.  
30  
31  
32  
33  
34  
35  
36  
37  
38  
39  
40  
41  
42  
43  
44  
45  
46  
47  
48  
49

50 The PAA [poly(acrylic acid), M.W. ~1800, Sigma Aldrich] functionalized cerium oxide  
51 nanoparticles (PNC) were synthesized as in Wu *et al.*<sup>24</sup> with modifications to control negatively  
52 charged PNC size. For PNC2, 0.217 g of  $\text{Ce}(\text{NO}_3)_3 \cdot 6\text{H}_2\text{O}$  (cerium (III) nitric hexahydrate, 99%,  
53 Aldrich) in 0.5 mL of molecular water was mixed with 0.450 g of PAA in another 0.5 mL of  
54  
55  
56  
57  
58  
59  
60



1  
2  
3 molecular water. The mixture was then added into 3 mL of  $\text{NH}_3 \cdot \text{H}_2\text{O}$  while vigorously stirring.  
4 For PNC11, 0.217 g of  $\text{Ce}(\text{NO}_3)_3 \cdot 6\text{H}_2\text{O}$  in 0.5 mL of molecular water was added rapidly into 3  
5 mL of  $\text{NH}_3 \cdot \text{H}_2\text{O}$  while vigorously stirring. After 1 min, 0.450 g of PAA in 0.5 mL of molecular  
6 water was added to the mixture. For PNC16, 0.217 g of  $\text{Ce}(\text{NO}_3)_3 \cdot 6\text{H}_2\text{O}$  in 0.5 mL of molecular  
7 water was added slowly (60s) into 3 mL of  $\text{NH}_3 \cdot \text{H}_2\text{O}$  while vigorously stirring. After 1 min,  
8 0.450 g of PAA in 0.5 mL of molecular water was added to the mixture. All the mixtures were  
9 kept stirring for 24 h before centrifugation to remove large aggregates, which was followed by  
10 purification with centrifugation filters (Amicon cell, MWCO 10k, Millipore Inc.) for 5 times at  
11 4,500 rpm.  
12  
13  
14  
15  
16  
17  
18  
19

20 To synthesize positively charged aminated dextran functionalized cerium oxide nanoparticles  
21 (ADNCs), dextran functionalized cerium oxide nanoparticles (DNCs) were prepared by  
22 following protocols in Asati *et al.*<sup>132</sup> with modifications, followed by functionalization with  
23 DEAE in NaOH solution.<sup>133</sup> For DNC8, 0.217 g of  $\text{Ce}(\text{NO}_3)_3 \cdot 6\text{H}_2\text{O}$  in 0.5 mL of molecular  
24 water was mixed with 1.010 g dextran (M.W. ~6,000, Alfa Aesar) in 0.5 mL of molecular water.  
25 For DNC12, 0.217 g of  $\text{Ce}(\text{NO}_3)_3 \cdot 6\text{H}_2\text{O}$  in 0.5 mL DI water was mixed with 0.450 g dextran in  
26 0.5 mL DI water. These solutions were separately added into 3 mL of  $\text{NH}_3 \cdot \text{H}_2\text{O}$  while vigorously  
27 stirring for 24 h. Centrifugation was used to remove large aggregates before purification with  
28 centrifugation filters (Amicon cell MWCO 10k, Millipore Inc.) for 5 times at 4,500 rpm. The  
29 purified DNC8 and DNC12 were redissolved in 10 mL of molecular water and mixed with 10  
30 mL of NaOH solution (80 mg/mL). Then 2.40 g of DEAE·HCl (diethylaminoethyl  
31 hydrochloride, 99.5%, Acros) was added to the mixture while vigorously stirring. The mixtures  
32 were stirred overnight before purification to remove unreacted free reagents and side products by  
33 centrifugation using centrifugation filters (Amicon cell MWCO 10k, Millipore Inc.) to yield  
34 ADNC8 and ADNC12.  
35  
36  
37  
38  
39  
40  
41  
42  
43  
44  
45  
46  
47

48 To label cerium oxide nanoparticles with DiI ((Z)-2-[(E)-3-(3,3-dimethyl-1-octadecylindol-1-  
49 ium-2-yl) prop-2-enylidene] -3,3-dimethyl-1-octadecylindole perchlorate, Invitrogen), the  
50 hydrophobic fluorescent dye was encapsulated and stabilized in the polymer coating (PAA or  
51 dextran) in PNCs and ADNCs following Asati *et al.*<sup>134</sup> Briefly, 4 mL of PNCs or ADNCs  
52 aqueous solution (1.5 mg/mL) was added to 0.2 mL of DiI solution (0.3 mg/mL) in DMSO  
53  
54  
55  
56  
57  
58  
59  
60

1  
2  
3 (Dimethyl sulfoxide, 99.9%, Fisher) while stirring at 1,000 rpm. After incubation overnight, the  
4 mixture was purified by centrifugation at 4,500 rpm using Amicon cell (MWCO 10k, Millipore  
5 Inc.) for 5 times to remove free DiI molecules from DiI labeled PNC and ADNC.  
6

7  
8 The negatively charged silica nanoparticles labeled with FITC (fluorescein isothiocyanate,  
9 Isomer I, 90%, Acros) were synthesized following the protocol reported by Larson *et al.*<sup>135</sup> with  
10 modifications. Briefly, FITC-silane compound was synthesized by reacting 3.9 mg of FITC with  
11 20  $\mu\text{L}$  of APTMS ((3-Aminopropyl)triethoxysilane, >97%, Aldrich) and forming a covalent  
12 isothioureia linkage in 80  $\mu\text{L}$  of ethanol and DMSO mixture (3:1, v/v). After half an hour, 10  $\mu\text{L}$   
13 of prepared FITC-saline compound solution was added into a solvent mixture with 9 mL of  
14 ethanol and 150  $\mu\text{L}$  molecular water and stirred at 500 rpm in a 50 mL falcon tube, followed by  
15 the addition of 350  $\mu\text{L}$  of TEOS (tetraethyl orthosilicate, 98%, Aldrich) and 100  $\mu\text{L}$  of  $\text{NH}_3 \cdot \text{H}_2\text{O}$   
16 in order. The mixture was kept stirred overnight in the dark before purification to remove  
17 unreacted free reagents by centrifugation using centrifugal filters (Amicon cell MWCO 10k,  
18 Millipore Inc.) to yield FITC-SN18.  
19  
20  
21  
22  
23  
24  
25  
26  
27  
28

### 29 **Nanoparticle characterization**

30 UV-vis spectra of nanoparticles were collected in a micro quartz cuvette (10 mm  $\times$  2 mm, path  
31 length 10 mm) using a Shimadzu UV-2600 spectrometer. Fluorescence emission spectra of  
32 nanoparticle samples were acquired with a PTI QuantaMaster 400 fluorometer in a quartz  
33 cuvette (10 mm  $\times$  10 mm). Fourier-transform infrared (FTIR) spectroscopy was performed with  
34 a Nicolet 6700 FTIR spectrometer. The size of nanoparticles was characterized with both  
35 dynamic light scattering (DLS) and transmission electron microscopy (TEM). DLS  
36 measurements were conducted with a Malvern Zetasizer Nano S. TEM was performed on a  
37 Philips FEI Tecnai 12 microscope operated at an accelerating voltage of 120 kV. The TEM  
38 samples were prepared by placing one drop of particle solution onto a Cu grid (400 mesh, Ted  
39 Pella) followed by drying at laboratory conditions. Zeta potential was measured with a Malvern  
40 Zetasizer Nano ZS with nanoparticles (0.1 mg/mL) dispersed in NaCl buffer (0.1 mM) and  
41 analyzed by the Hückel approximation. For a 0.1 mM aqueous solution, the Debye length ( $1/\kappa$ ) is  
42  $\sim 30$  nm. Thus, the Hückel approximation applies for all 10 types of nanoparticles in this study  
43 with size below 20 nm.<sup>136–138</sup> Because surfactant bubble formation interferes with DLS  
44 measurements, nanoparticle stability in surfactants was assessed by centrifugation. All  
45  
46  
47  
48  
49  
50  
51  
52  
53  
54  
55  
56  
57  
58  
59  
60

1  
2  
3 nanoparticles formulations were centrifuged at 13.2 k rpm for 15 min to determine potential  
4 aggregation, and no precipitates were observed for CDs, cerium oxide, and silica nanoparticles.  
5  
6

### 7 8 **Plant growth**

9  
10 Cotton seeds (*Gossypium hirsutum* L.) cultivar Acala 1517-08 were sterilized for 15 min in 9%  
11 H<sub>2</sub>O<sub>2</sub>, washed three times followed by 24 h imbibition in double distilled water, and then planted  
12 in the plastic pots (10×10×9 cm<sup>3</sup>) filled with standard soil mix (Sunshine, LC1 mix). Maize (*Zea*  
13 *mays* L., golden bantam) seeds were planted in the plastic pots (8.5×8.5×8.5 cm<sup>3</sup>) using the same  
14 soil described above. Cotton and maize plants were grown in a LED growth chamber (HiPoint)  
15 at 21/26 °C (day/night) with a 14 h photoperiod at photosynthetic active radiation (PAR) of 360  
16 to 450 and 200 to 250 μmol•m<sup>-2</sup>•s<sup>-1</sup>, respectively. Three-week-old cotton and 10-day-old maize  
17 seedlings were used in experiments for this study when plants were at the two true leaf stage.  
18  
19  
20  
21  
22  
23

### 24 25 **Leaf characterization**

26  
27 All leaves used in this study were the first true leaves of cotton and maize plants at the two-leaf  
28 stage. Scanning electron microscopy (SEM) of the leaf epidermis was performed with a Hitachi  
29 TM-1000 (Japan). SEM samples of cotton and maize leaves were cut into 1 cm<sup>2</sup> and immersed in  
30 isopentane (cooled by liquid nitrogen) for 5 s before placing them onto the sample stage for  
31 imaging. The SEM images were analyzed with ImageJ to measure stomatal densities and lengths.  
32 Leaf cross-section images were visualized under a microscope (BZ-X710, Keyence, Osaka,  
33 Japan). Leaf cross-section samples of cotton and corn leaves were embedded by 7% agarose,  
34 sectioned into 40 and 50 μm under an oscillating tissue slicer (EMS 500, Electron Microscopy  
35 Sciences Inc., and Hatfield, PA). Samples were stained with 0.01% Toluidine Blue O for 1 min,  
36 and washed gently with distilled water.<sup>139</sup> The leaf autofluorescence spectra were acquired with a  
37 PTI QuantaMaster 400 fluorometer with cotton or maize leaf mounted on a solid sample holder.  
38 Leaf chlorophyll content was quantified with a SPAD 502 plus chlorophyll meter (Konica  
39 Minolta, Tokyo, Japan) and measured as chlorophyll content index (CCI).  
40  
41  
42  
43  
44  
45  
46  
47  
48  
49  
50

### 51 52 **Composition and application of foliar nanoparticle formulations**

53 All nanoparticle formulations were composed of one surfactant (Silwet L-77, Bio World, 0.2 %  
54 applied for cotton or 0.3 % for maize, or Triton X-100, IBI Scientific, 0.2% for both cotton and  
55 maize) as a wetting agent. The surface tension of nanoparticle formulations was measured by the  
56  
57  
58  
59  
60

1  
2  
3 Wilhelmy plate method using a surface tensiometer (Kino, Model A3). Briefly, the platinum  
4 plate was cleaned with DI water and heated with an alcohol burner until the plate turned red  
5 (~30s) before it was hung onto the hook of the surface tensiometer. Nanoparticle formulation (5  
6 mL) was added into a clean glass sample container and placed on the surface tensiometer stage  
7 below but without touching the plate. After the tensiometer reading was stable, the sample stage  
8 was raised using a micrometer until the bottom of the plate is in contact with the surface of the  
9 formulation. At this point, the measured surface tension values from the tensiometer were  
10 recorded. We assessed if DiI and FITC fluorescent dyes dissociate from the nanoparticles in the  
11 presence of surfactants. The DiI-PNC2, DiI-ADNC12, and FITC-SN18 were suspended in Silwet  
12 L-77 formulations, and centrifuged at 4500 rpm for 30 min in Amicon cell centrifugal filters  
13 (MWCO 3k, Millipore Inc.). UV-vis spectrophotometry was used to detect potential absorbance  
14 peaks for DiI or FITC dyes. A humectant (glycerol, 3%) was also included in formulations to  
15 improve attachment and retention of the applied formulations on the maize leaf surface (Figure  
16 S22). The nanoparticle concentrations were selected based on optimization of fluorescence signal  
17 for imaging by confocal microscopy and maintenance of leaf health upon nanoparticle exposure.  
18 The concentrations of CDs were 0.5 and 5 mg/mL for cotton and maize, respectively. The  
19 concentration of the cerium oxide nanoparticles and silica nanoparticles were 0.5 mg/mL for  
20 both cotton and maize. Non-surfactant formulation controls containing CDs (PEI-CD2 and SA-  
21 CD2) at the same concentrations and volumes as those with surfactants were applied to cotton  
22 and maize leaves while mounted on a flat surface to prevent non-surfactant formulation from  
23 dripping off the leaf surface. Cotton and maize leaves were in the dark during application of  
24 nanoparticles onto the whole surface of the first true leaf.  
25  
26  
27  
28  
29  
30  
31  
32  
33  
34  
35  
36  
37  
38  
39  
40  
41  
42

### 43 **Confocal microscopy imaging of nanoparticles in leaves**

44 Leaves were imaged by using an inverted Leica TCS-SP5 spectral confocal laser scanning  
45 microscope from the leaf epidermis, where higher nanoparticle fluorescence signals were  
46 detected, and into the leaf mesophyll. Samples were mounted on microscope slides (Corning  
47 2948-75X25) having a Carolina observation gel chamber (~1 mm in thickness) made with a cork  
48 borer (diameter, 8 mm). A leaf disk was taken from a treated leaf with a cork borer (diameter, 6  
49 mm), immersed in the chamber filled with perfluorodecalin (PFD, 90%, Acros) and sealed with a  
50 coverslip (VWR). Leaf disks from non-surfactant formulation controls were taken right  
51  
52  
53  
54  
55  
56  
57  
58  
59  
60

1  
2  
3 underneath the site of application. Confocal microscopy imaging settings were as follows: 40×  
4 wet objective (HCX PL APO CS 40.0x1.10 WATER UV, Leica Microsystems, Germany); laser  
5 excitation 405 nm, 514 nm, and 476 nm for samples treated with CDs, NCs, and FITC-SN18,  
6 respectively; z-stack section thickness = 2 μm; line average = 4; PMT1 (NP channel), 410–490,  
7  
8 respectively; z-stack section thickness = 2 μm; line average = 4; PMT1 (NP channel), 410–490,  
9  
10 550–615, or 500–600 nm for samples treated with CDs, NCs, or FITC-SN18, respectively;  
11  
12 PMT2 (chlorophyll channel), 700–790 nm. The x-y resolution based on the 40× objective  
13  
14 numerical aperture (NA=1.1) and laser wavelengths 405, 476, and 514 nm was calculated at 225,  
15  
16 264, 285 nm, respectively, using the equation  $d=0.61\lambda/NA$ , where d is resolution and  $\lambda$  is the  
17  
18 light wavelength. At least five cotton or maize plants were used for confocal microscopy  
19  
20 imaging from the leaf epidermis into the mesophyll cells. Representative confocal microscopy  
21  
22 images of nanoparticle treatments (Figure 5 and S16-S19), and control leaf samples exposed to  
23  
24 surfactant alone are shown (Figure S23). Guard cell and NP colocalization was determined by  
25  
26 analyzing confocal images as follows. The total number of guard cells were counted in the  
27  
28 confocal microscopy images on the leaf epidermis, where all guard cells were outlined by the  
29  
30 fluorescence of foliarly applied nanoparticles. Guard cells with nanoparticles inside were  
31  
32 identified through confocal microscopy z-stacks from the leaf epidermis into the mesophyll. The  
33  
34 colocalization rates were calculated as the percentage of guard cell pairs with nanoparticle  
35  
36 fluorescence relative to total number of guard cell pairs. Colocalization of leaf extracellular  
37  
38 space and NPs was determined in confocal images in which mesophyll cell boundaries were  
39  
40 delineated by chloroplasts localized at the plant cell membrane due to exposure to laser  
41  
42 excitation during confocal microscopy imaging.<sup>111–113</sup> Fluorescent dyes were not used to label  
43  
44 plant cell boundaries because they quench CD fluorescence. Instead chloroplasts were used to  
45  
46 delineate the plasma membrane boundary in leaf mesophyll cells upon laser excitation as  
47  
48 reported previously.<sup>111–113</sup> This was confirmed in cotton and maize leaves by imaging  
49  
50 chloroplasts in cells with cell membranes stained by FM 1-43 fluorescent dye (Figure S21).  
51  
52 Cotton and maize leaves were infiltrated with FM 1-43 (10 μg/mL) in TES buffer (10 mM) to  
53  
54 stain cell membranes<sup>140–142</sup> using a needleless syringe (1 mL) and incubated for 10 min. Leaf  
55  
56 disks were taken for confocal microscopy imaging using 40× wet objective (HCX PL APO CS  
57  
58 40.0×1.10 WATER UV, Leica Microsystems, Germany); laser excitation 405, 476, or 514 nm,  
59  
60 respectively; z-stack section thickness = 2 μm; line average = 4; PMT1 (FM1-43 channel), 520–  
620 nm; PMT2 (chlorophyll channel), 700–790 nm. All pixels inside the cells were removed

1  
2  
3 using ImageJ to obtain the extracellular space. The extracellular space and NP colocalization was  
4 calculated as the area occupied by NPs in the extracellular space divided by the whole area of  
5 extracellular space. Colocalization between NPs and chloroplasts was analyzed with LAS (Leica  
6 Application Suite) AF Lite software. Six line sections were drawn across the so-called “region of  
7 interest” (ROI) with 30  $\mu\text{m}$  interval on the confocal images. The corresponding distribution  
8 profiles of fluorescence intensity of NPs and chloroplast autofluorescence for each ROI line were  
9 plotted. The colocalization rate of chloroplasts with NPs was counted as the proportion of  
10 chloroplast pigment fluorescence emission peaks which are overlapped with NP fluorescence  
11 peaks out of all chloroplast peaks. We only counted chloroplast emission peaks fully overlapped  
12 with NP emission peaks and excluded partially overlapped peaks to eliminate potential false  
13 positive colocalization due to the confocal imaging resolution limit. Nanoparticle overlay with  
14 chloroplast and guard cell edges within the x-y resolution was not considered as colocalization  
15 with these plant structures.  
16  
17  
18  
19  
20  
21  
22  
23  
24  
25  
26

27 High spatial and temporal resolution confocal images of CDs entering cotton and maize leaves *in*  
28 *planta* were acquired with an upright Zeiss 880 confocal laser scanning microscope using a 40  $\times$   
29 water dipping objective (LD LCI Plan-Apochromat 40 $\times$ /1.2 Imm Corr DIC M27). Plants were  
30 taken out from pots carefully with the soil attached on their roots to avoid root damage.  
31 Immediately, the plant roots were covered with moist paper towels, plastic film, and foil. The  
32 first true leaves were mounted onto microscope slides and secured with double-sided tape.  
33 Coverslips were then placed over the leaves and mounted to microscope slides with super glue,  
34 so that a narrow space was left between the coverslip and the leaves for delivering the CD  
35 formulation. Formulations without CDs were applied first to record control z-stack images in flat  
36 scanning areas on the leaf surface where both leaf mesophyll cells and stomata were previously  
37 identified. Then a CD formulation was added and the z-stack images were taken continuously  
38 with section thickness of 2  $\mu\text{m}$  and a scanning cycle about 2 to 5 mins depending on the z-stack  
39 layers. The formulation without nanoparticles was added every 15 min to keep the liquid layer in  
40 between the microscopy slide and the leaf lamina. Samples were excited with 405 nm (6.0%) and  
41 458 nm (1.0%) laser lines, with an emission band recorded at 410-490 nm for CDs and 700-758  
42 nm for chlorophyll autofluorescence. The x-y resolution based on the 40 $\times$  objective (NA=1.2)  
43 and laser wavelengths 405 and 458 nm was calculated at 206 and 233 nm, respectively, using the  
44  
45  
46  
47  
48  
49  
50  
51  
52  
53  
54  
55  
56  
57  
58  
59  
60

1  
2  
3 equation  $d=0.61\lambda/NA$ , where  $d$  is resolution and  $\lambda$  is the light wavelength. ImageJ was used to  
4 reconstruct 3D images and videos of CDs in leaves (Video S1-S8).  
5  
6  
7

### 8 **Statistical analysis**

9  
10 Statistical analysis was performed in SPSS 20.0 software (IBM, New York, USA). Zeta potential  
11 comparisons and nanoparticle colocalization differences in guard cells, extracellular space and  
12 chloroplasts were analyzed by nonparametric independent samples Kruskal-Wallis one-way  
13 ANOVA test. Calculation of efficient delivery regions based on confidence ellipse analysis<sup>143,144</sup>  
14 were possible only for plant cell compartments having three or more efficient combinations of  
15 nanoparticle size and charge. The ellipse parameters were calculated based on the hydrodynamic  
16 size and zeta potential of nanoparticles with above average delivery efficiency to guard cells,  
17 chloroplasts and extracellular space (Table S2). The ellipse center coordinates are means of  
18 hydrodynamic size and zeta potential, and ellipse axes lengths and rotation angle were calculated  
19 based on confidence levels and the covariance matrix of hydrodynamic size and zeta potential of  
20 nanoparticles (Table S2).  
21  
22  
23  
24  
25  
26  
27  
28  
29  
30

### 31 **Supporting Information.**

32  
33  
34 The Supporting Information is available free of charge on the ACS Publications website at DOI:  
35 xxxxxxxx.  
36  
37  
38

- 39 ● **Figures S1 to S23.** Stomatal density and length of cotton and maize, leaf autofluorescence  
40 of cotton and maize, TEM images, FTIR and UV/vis spectra of nanoparticles, surface  
41 tension and pH values of nanoparticle formulations, representative confocal images for  
42 assessing leaf uptake of PEI-CD2 and SA-CD2 in cotton and maize leaves with Triton X-  
43 100 or Silwet L-77 as surfactant or in water formulation without surfactant, 3D  
44 renderings of confocal microscopy images showing nanoparticle delivery pathways from  
45 the leaf surface into mesophyll cells of cotton and maize, images of nanoparticle  
46 suspensions indicating high stability in surfactant formulation, UV-vis absorption spectra  
47 showing no fluorescent dye leaking from nanoparticles in the presence of Silwet L-77,  
48 leaf chlorophyll content patterns in cotton and maize after exposure to foliar topical  
49  
50  
51  
52  
53  
54  
55  
56  
57  
58  
59  
60

1  
2  
3 formulations (CDs) with Silwet L-77 as surfactants, high spatial and temporal resolution  
4 images of nanoparticle translocation pathways from the leaf surface into the mesophyll,  
5 confocal microscopy images with higher magnification of cotton and maize leaf  
6 mesophyll cells after foliar delivery of 10 types of nanoparticles suspended in  
7 formulation of Silwet L-77 as surfactant, positive linear correlation between  
8 colocalization rate of chloroplasts based on ROI analysis and Manders' overlap  
9 coefficient, representative confocal microscopy images of chloroplast autofluorescence  
10 and leaf mesophyll cells with FM 1-43 fluorescent dye, positive linear correlation  
11 between extracellular space area determined by chloroplast autofluorescence arrangement  
12 *versus* FM 1-43 labeled cell membranes, representative confocal images indicating  
13 colocalization of chloroplast autofluorescence with foliar-applied nanoparticles (PEI-  
14 CD6) using formulations with or without humectant (glycerol, 3%), representative  
15 confocal images showing no nanoparticle fluorescence when leaves were treated with  
16 control formulations without nanoparticles for cotton and maize.

- 17 ● Table S1 and S2. Hydrodynamic size (average  $\pm$  standard deviation, nm) and zeta  
18 potential (average  $\pm$  standard deviation, mV) of nanoparticles, and confidence ellipse  
19 equation with corresponding parameters for determining nanoparticle efficient delivery  
20 regions.
- 21 ● Video S1 to S16. Time-lapse videos showing uptake of CDs by cotton and maize leaves  
22 *in planta*, videos of reconstructed 3D confocal images of CD distribution in cotton and  
23 maize leaf tissues.

## 41 ORCID

42 Peiguang Hu: 0000-0002-9526-6295

43 Juan Pablo Giraldo: 0000-0002-8400-8944

## 44 Author Contributions

45 P.H. and J.A. contributed equally. J.P.G., P.H., and J.A. conceived and designed this study. P.H.,  
46 J.A., and M.F. performed experiments. P.H., J.A., J.P.G., and H.W. analyzed the results. J.P.G.,  
47  
48  
49



1  
2  
3 P.H., J.A., H.W., X.T., and Z.L. wrote the manuscript. All authors have read and agreed with the  
4 manuscript.  
5  
6

## 7 **Current Address**

8  
9  
10 †College of Plant Science & Technology, Huazhong Agricultural University, Wuhan 430070,  
11  
12 China  
13  
14  
15

## 16 **Conflict of Interest**

17  
18  
19  
20 The authors declare no competing financial interests.  
21  
22

## 23 **Acknowledgments**

24  
25  
26  
27 This work was supported by the National Science Foundation under the Center for Sustainable  
28 Nanotechnology, CHE-1503408. The CSN is part of the Centers for Chemical Innovation  
29 Program. Transmission Electron microscopy was performed on a TEM FEI Tecnai 12 in Central  
30 Facility for Advanced Microscopy and Microanalysis (CFAMM) at UC Riverside. Cotton seeds  
31 Acala 1517-08 were provided by Prof. Jinfa Zhang from the Department of Plant and  
32 Environmental Sciences, New Mexico State University. Jing An acknowledges funds from a  
33 Chinese Scholarship Council Fellowship.  
34  
35  
36  
37  
38  
39

## 40 **Figure Legends**

41  
42  
43  
44 **Figure 1. Nanoparticle translocation pathways and distribution in plant leaves with**  
45 **different anatomical properties. a,** Nanoparticles (*e.g.* CDs, CeO<sub>2</sub> and SiO<sub>2</sub>) translocate across  
46 the leaf epidermal barrier either through stomatal (red line) and/or cuticular (pink line) pathways,  
47 then move through the extracellular space and in between cell walls (apoplastic pathway) and/or  
48 enter the leaf mesophyll cells and translocate between cells through the cytosol (symplastic  
49 pathway). The translocation pathways are influenced by the differences in anatomical properties  
50 between dicot (cotton) and monocot (maize) plant leaves. Nanoparticles can localize in leaf cells  
51  
52  
53  
54  
55  
56  
57  
58  
59  
60

1  
2  
3 in the epidermis (*e.g.* guard cells), extracellular space, or organelles (*e.g.* chloroplasts). **b**,  
4 Representative SEM images of cotton and maize leaf epidermal surfaces indicating differences in  
5 stomatal arrangement, density, and length. **c**, Brightfield images of leaf cross-sections  
6 highlighting the differences in anatomy of leaf epidermal and mesophyll tissues in dicot (cotton)  
7 and monocot (maize) plant species. Arrows point to guard cells (red), extracellular space (cyan),  
8 and chloroplast (green).  
9

10  
11  
12  
13  
14 **Figure 2. Design and characterization of nanoparticle chemical and physical properties for**  
15 **understanding their interactions with leaf cell and organelles.** **a**, Carbon dots (PEI-CDs and  
16 SA-CDs), CeO<sub>2</sub> (DiI-PNCs and DiI-ADNCs), and SiO<sub>2</sub> (FITC-SN) nanoparticles were  
17 synthesized with hydrodynamic diameters, measured by DLS, from 1.7-18 nm. **b**, Surface  
18 chemical modifications were used to generate hydrophilic nanoparticles with highly positive or  
19 negative zeta potential for understanding the role of charge in determining translocation through  
20 plant surfaces including the leaf cell walls, cell and organelle lipid bilayers, Mean  $\pm$  SD. Zeta  
21 potential comparisons were analyzed by Kruskal-Wallis one-way ANOVA tests. Different  
22 lowercase letters indicate significant differences ( $P < 0.05$ ). **c**, Nanoparticle optical properties  
23 were designed to optimize the fluorescence signal in the visible window within the range of low  
24 leaf background fluorescence emission for cotton and maize. Excitation wavelengths: 405 nm for  
25 leaves, PEI-CDs and SA-CDs; 514 nm for DiI-PNCs and DiI-ADNCs; and 476 nm for FITC-  
26 SN18. PEI-CDs, branched polyethyleneimine coated carbon dots; SA-CDs, succinic anhydride  
27 modified PEI-CDs; DiI-PNCs, poly(acrylic acid) coated cerium oxide nanoparticles labeled with  
28 DiI as fluorescent dye; DiI-ADNCs, aminated dextran coated cerium oxide nanoparticles labeled  
29 with DiI as fluorescent dye; FITC-SN18, silica nanoparticles labeled with FITC as fluorescent  
30 dye. Last digits in nanoparticle labels indicate hydrodynamic size, for example, PEI-CD2 (PEI-  
31 CD with hydrodynamic size about 2 nm).  
32  
33  
34  
35  
36  
37  
38  
39  
40  
41  
42  
43  
44  
45  
46

47 **Figure 3. Formulations with low surface tension enable nanoparticle foliar delivery into**  
48 **plant leaves.** **a**, Comparison of foliar delivery of CDs suspended in formulations with low *versus*  
49 high surface tension using the surfactants Silwet L-77 (~22 mN/m) and Triton X-100 (~30  
50 mN/m), respectively. Positively and negatively CDs of different sizes (PEI-CD2 (1.7 nm), SA-  
51 CD2 (1.9 nm), PEI-CD6 (5.5 nm), and SA-CD6 (6.4 nm)) were imaged by confocal microscopy  
52 to determine nanoparticle leaf uptake, n=5. **b**, Representative confocal fluorescence microscopy  
53  
54  
55  
56  
57  
58  
59  
60

1  
2  
3 images (2  $\mu\text{m}$  z-axis, and 225 - 285 nm x-y resolution, Leica SP5) of the leaf mesophyll (cotton  
4 and maize) indicating leaf translocation of CDs larger than 5 nm (PEI-CD6 (5.5 nm), SA-CD6  
5 (6.4 nm)) when nanoparticles are delivered in Silwet L-77. However, no CDs above 5 nm were  
6 observed inside leaves when the nanoparticles were delivered with Triton X-100. n=5, Mean  $\pm$   
7 SD. Images were collected after 3h incubation with nanoparticles. NP and Chl represent  
8 nanoparticles (green) and chloroplasts (magenta), respectively. The (+) and (-) indicate positively  
9 and negatively charged nanoparticles, respectively.  
10  
11  
12  
13  
14  
15  
16

17 **Figure 4. High spatial and temporal resolution imaging of nanoparticle translocation**  
18 **pathways from the leaf surface into the mesophyll *in planta*.** Snapshots from confocal  
19 fluorescence microscopy videos showing pathways of CD movement (2 nm in size, green) in  
20 real-time (3.5 and 1.7 min resolution for cotton and maize, respectively) from the leaf surface  
21 into mesophyll cells and chloroplasts (magenta) (Video S1 and S2). In cotton, the CDs move  
22 through both cuticular and stomatal pathways through the leaf epidermis, whereas in maize the  
23 CDs penetrate the leaf surface mainly through the stomatal pathway. In both species, CDs  
24 delivered in Silwet L-77 move rapidly from the leaf epidermis into the mesophyll within 10-20  
25 min. Arrows point to the stomatal pathways (white), and cuticular pathways (yellow). t=0 min  
26 represents images captured before nanoparticle formulation was added. 2  $\mu\text{m}$  z-axis resolution,  
27 206 - 233 nm x-y resolution (Zeiss 880).  
28  
29  
30  
31  
32  
33  
34  
35  
36  
37

38 **Figure 5. Nanoparticle distribution in leaf cells and organelles.** **a**, Representative confocal  
39 fluorescence microscopy images of foliar-delivered nanoparticles (green) to different tissue and  
40 cell compartments in cotton and maize leaves including chloroplasts (white arrows), extracellular  
41 space (cyan arrows), and stomatal guard cells (yellow arrows). Orthogonal views of  
42 representative confocal microscopy z-stacks displaying the colocalization of nanoparticles in **b**,  
43 chloroplasts with corresponding line transect colocalization analysis of nanoparticle and  
44 chloroplast fluorescence peak overlap, **c**, extracellular space, and **d**, stomatal guard cells (red  
45 arrow) and stomatal pores (orange arrow). 2  $\mu\text{m}$  z-axis resolution, 225 - 285 nm x-y resolution  
46 (Leica SP5). Images were collected after 3h incubation with nanoparticles. NP and Chl represent  
47 nanoparticles (green) and chloroplasts (magenta), respectively. The (+) and (-) indicate positively  
48 and negatively charged nanoparticles, respectively.  
49  
50  
51  
52  
53  
54  
55  
56  
57  
58  
59  
60

1  
2  
3  
4  
5 **Figure 6. Nanoparticle-Leaf interaction (NLI) empirical models for designing nanoparticle**  
6 **charge and size with improved delivery efficiency to specific leaf cells and organelles.** Box  
7 plots of colocalization rates for positively and negatively charged nanoparticles ranging from  
8 1.7-18 nm in size with **a**, guard cells in the leaf epidermis, **b**, extracellular space, and **c**,  
9 chloroplasts in the leaf mesophyll of cotton (left column) and maize (right column). Boxes  
10 represent the interquartile range from the first to the third quartile with squares as the medians;  
11 minimum and maximum values (snapped to mean  $- 1 \times$  SD and mean  $+ 1 \times$  SD, SD = standard  
12 deviation) are shown with whiskers; red or blue circles are actual data points. Dotted lines  
13 represent the averages (grey) and standard errors (SE, black) of all non-zero data points.  
14 Nanoparticles with efficient delivery to guard cells, extracellular space, or chloroplasts are those  
15 with colocalization rates in the region above these averages minus SE (lower dotted black line).  
16 Nanoparticle colocalization differences in guard cells, extracellular space and chloroplasts were  
17 analyzed by Kruskal-Wallis one-way ANOVA. Different lowercase letters indicate significant  
18 differences ( $P < 0.05$ ). **d**, NLI empirical models represented by 95% (dashed lines) and 90%  
19 (dash-dotted lines) confidence ellipses, indicating the size and zeta potential regions with  
20 predicted above average nanoparticle delivery efficiency to leaf guard cells, chloroplasts, and  
21 extracellular space.  
22  
23  
24  
25  
26  
27  
28  
29  
30  
31  
32  
33  
34  
35

## 36 References

- 37  
38  
39  
40 (1) Alexandratos, N.; Bruinsma, J. World Agriculture towards 2030/2050: The 2012 Revision, 2012.  
41 Food and Agriculture Organization of the United Nations. <http://www.fao.org/3/a-ap106e.pdf>  
42 (accessed May 17, 2019)
- 43 (2) The Future of Food and Agriculture: Trends and Challenges, 2018. Food and Agriculture  
44 Organization of the United Nations. <http://www.fao.org/3/a-i6583e.pdf> (accessed May. 9, 2019)
- 45 (3) White, J. C.; Gardea-Torresdey, J. Achieving Food Security through the Very Small. *Nat.*  
46 *Nanotechnol.* **2018**, *13*, 627–629.
- 47 (4) Ray, D. K.; Mueller, N. D.; West, P. C.; Foley, J. A. Yield Trends Are Insufficient to Double Global  
48 Crop Production by 2050. *PLoS One* **2013**, DOI.org/10.1371/journal.pone.0066428.
- 49 (5) Kah, M.; Tufenkji, N.; White, J. C. Nano-Enabled Strategies to Enhance Crop Nutrition and  
50 Protection. *Nat. Nanotechnol.* **2019**, *14*, 532–540.
- 51 (6) Climate Impacts on Agriculture and Food Supply, 2016. The United States Environmental Protection  
52 Agency. [https://19january2017snapshot.epa.gov/climate-impacts/climate-impacts-agriculture-and-](https://19january2017snapshot.epa.gov/climate-impacts/climate-impacts-agriculture-and-food-supply_.html)  
53 [food-supply\\_.html](https://19january2017snapshot.epa.gov/climate-impacts/climate-impacts-agriculture-and-food-supply_.html) (accessed May 9, 2019).
- 54 (7) Schlenker, W.; Lobell, D. B. Robust Negative Impacts of Climate Change on African Agriculture.  
55 *Environ. Res. Lett.* **2010**, *5*, 014010.  
56  
57  
58  
59  
60

- 1  
2  
3 (8) Piao, S.; Ciais, P.; Huang, Y.; Shen, Z.; Peng, S.; Li, J.; Zhou, L.; Liu, H.; Ma, Y.; Ding, Y.;  
4 Friedlingstein, P.; Liu, C.; Tan, K.; Yu, Y.; Zhang, T.; Fang, J. The Impacts of Climate Change on  
5 Water Resources and Agriculture in China. *Nature* **2010**, *467*, 43–51.
- 6 (9) Ladha, J. K.; Pathak, H.; J. Krupnik, T.; Six, J.; van Kessel, C. Efficiency of Fertilizer Nitrogen in  
7 Cereal Production: Retrospects and Prospects *Adv. Agron.* **2005**, *87*, 85–156
- 8 (10) van de Wiel, C. C. M.; van der Linden, C. G.; Scholten, O. E. Improving Phosphorus Use Efficiency  
9 in Agriculture: Opportunities for Breeding. *Euphytica* **2016**, *207*, 1–22.
- 10 (11) Syers, K.; Johnston, E.; Curtin, D. A New Perspective on the Efficiency of Phosphorus Fertilizer  
11 Use. *19th World Congress of Soil Science, Soil Solutions for a Changing World*; Brisbane, Australia;  
12 August 1–6, 2010; pp 1–3.
- 13 (12) Aktar, M. W.; Sengupta, D.; Chowdhury, A. Impact of Pesticides Use in Agriculture: Their Benefits  
14 and Hazards. *Interdiscip. Toxicol.* **2009**, *2*, 1–12.
- 15 (13) Mahvi, A. H.; Nouri, J.; Babaei, A. A.; Nabizadeh, R. Agricultural Activities Impact on  
16 Groundwater Nitrate Pollution. *Int. J. Environ. Sci. Tech.* **2005**, *2*, 41–47.
- 17 (14) Wimalawansa, S. A.; Wimalawansa, S. J. Agrochemical-Related Environmental Pollution: Effects  
18 on Human Health. *Global J. Biol. Agric. Health Sci.* **2014**, *3*, 72–83.
- 19 (15) Md. Muhibbullah; Salma Momotaz; A.T. Chowdhury. Use of Agrochemical Fertilizers and Their  
20 Impact on Soil, Water and Human Health in the Khamargao Village of Mymensingh District,  
21 Bangladesh. *J. Agron.* **2005**, *4*, 109–115.
- 22 (16) Duhan, J. S.; Kumar, R.; Kumar, N.; Kaur, P.; Nehra, K.; Duhan, S. Nanotechnology: The New  
23 Perspective in Precision Agriculture. *Biotechnol Rep (Amst)* **2017**, *15*, 11–23.
- 24 (17) Raliya, R.; Saharan, V.; Dimkpa, C.; Biswas, P. Nanofertilizer for Precision and Sustainable  
25 Agriculture: Current State and Future Perspectives. *J. Agric. Food Chem.* **2018**, *66*, 6487–6503.
- 26 (18) Chen, H.; Yada, R. Nanotechnologies in Agriculture: New Tools for Sustainable Development.  
27 *Trends Food Sci. Technol.* **2011**, *22*, 585–594.
- 28 (19) Marchiol, L. Nanotechnology in Agriculture: New Opportunities and Perspectives. In *New Visions in*  
29 *Plant Science*; Çelik, Ö., Ed.; InTech: London, 2018; pp 121–142.
- 30 (20) Sangeetha, J.; Thangadurai, D.; Hospet, R.; Purushotham, P.; Karekalammanavar, G.; Mundaragi, A.  
31 C.; David, M.; Shinge, M. R.; Thimmappa, S. C.; Prasad, R.; Harish, E. R. Agricultural  
32 Nanotechnology: Concepts, Benefits, and Risks. In *Nanotechnology: An Agricultural Paradigm*;  
33 Prasad, R., Kumar, M., Kumar, V., Eds.; Springer Singapore: Singapore, 2017; pp 1–17.
- 34 (21) Kaushal, M.; Wani, S. P. Nanosensors: Frontiers in Precision Agriculture. In *Nanotechnology: An*  
35 *Agricultural Paradigm*; Prasad, R., Kumar, M., Kumar, V., Eds.; Springer Singapore: Singapore,  
36 2017; pp 279–291.
- 37 (22) Wu, H.; Shabala, L.; Shabala, S.; Giraldo, J. P. Hydroxyl Radical Scavenging by Cerium Oxide  
38 Nanoparticles Improves *Arabidopsis* Salinity Tolerance by Enhancing Leaf Mesophyll Potassium  
39 Retention. *Environ. Sci.: Nano* **2018**, *5*, 1567–1583.
- 40 (23) Djanaguiraman, M.; Nair, R.; Giraldo, J. P.; Prasad, P. V. V. Cerium Oxide Nanoparticles Decrease  
41 Drought-Induced Oxidative Damage in Sorghum Leading to Higher Photosynthesis and Grain Yield.  
42 *ACS Omega* **2018**, *3*, 14406–14416.
- 43 (24) Wu, H.; Tito, N.; Giraldo, J. P. Anionic Cerium Oxide Nanoparticles Protect Plant Photosynthesis  
44 from Abiotic Stress by Scavenging Reactive Oxygen Species. *ACS Nano* **2017**, *11*, 11283–11297.
- 45 (25) Lawrence, J. R.; Swerhone, G. D. W.; Dynes, J. J.; Hitchcock, A. P.; Korber, D. R. Complex Organic  
46 Corona Formation on Carbon Nanotubes Reduces Microbial Toxicity by Suppressing Reactive  
47 Oxygen Species Production. *Environ. Sci.: Nano* **2016**, *3*, 181–189.
- 48 (26) Tourinho, P. S.; Van Gestel, C. A. M.; Lofts, S.; Svendsen, C.; Soares, A. M.; Loureiro, S. Metal-  
49 Based Nanoparticles in Soil: Fate, Behavior, and Effects on Soil Invertebrates. *Environ. Toxicol.*  
50 *Chem.* **2012**, *31*, 1679–1692.
- 51 (27) Ma, J. F. Role of Silicon in Enhancing the Resistance of Plants to Biotic and Abiotic Stresses. *Soil*  
52 *Sci. Plant Nutr.* **2004**, *50*, 11–18.
- 53 (28) Wong, M. H.; Misra, R. P.; Giraldo, J. P.; Kwak, S.-Y.; Son, Y.; Landry, M. P.; Swan, J. W.;
- 54  
55  
56  
57  
58  
59  
60

- Blankschtein, D.; Strano, M. S. Lipid Exchange Envelope Penetration (LEEP) of Nanoparticles for Plant Engineering: A Universal Localization Mechanism. *Nano Lett.* **2016**, *16*, 1161–1172.
- (29) Giroto, A. S.; Guimarães, G. G. F.; Foschini, M.; Ribeiro, C. Role of Slow-Release Nanocomposite Fertilizers on Nitrogen and Phosphate Availability in Soil. *Sci. Rep.* **2017**, *7*, 46032.
- (30) El-Aila, H. I.; El-Sayed, S. A. A.; Yassen, A. A. Response of Spinach Plants to Nanoparticles Fertilizer and Foliar Application of Iron. *Int. J. Environ* **2015**, *4*, 181–185.
- (31) Singh, A.; Bhati, A.; Tripathi, K. M.; Sonkar, S. K. Nanocarbons in Agricultural Plants: Can Be a Potential Nanofertilizer? In *Nanotechnology in Environmental Science*; Hussain, C. M., Mishra, A. K., Eds; Wiley-VCH: Weinheim, Germany, 2018; pp 153–190.
- (32) Kah, M. Nanopesticides and Nanofertilizers: Emerging Contaminants or Opportunities for Risk Mitigation? *Front Chem* **2015**, *3*, 64.
- (33) Li, J.; Wu, H.; Santana, I.; Fahlgren, M.; Giraldo, J. P. Standoff Optical Glucose Sensing in Photosynthetic Organisms by a Quantum Dot Fluorescent Probe. *ACS Appl. Mater. Interfaces* **2018**, *10*, 28279–28289.
- (34) Giraldo, J. P.; Landry, M. P.; Faltermeier, S. M.; McNicholas, T. P.; Iverson, N. M.; Boghossian, A. A.; Reuel, N. F.; Hilmer, A. J.; Sen, F.; Brew, J. A.; Strano, M. S. Plant Nanobionics Approach to Augment Photosynthesis and Biochemical Sensing. *Nat. Mater.* **2014**, *13*, 400–408.
- (35) Giraldo, J. P.; Landry, M. P.; Kwak, S.-Y.; Jain, R. M.; Wong, M. H.; Iverson, N. M.; Ben-Naim, M.; Strano, M. S. A Ratiometric Sensor Using Single Chirality Near-Infrared Fluorescent Carbon Nanotubes: Application to *In Vivo* Monitoring. *Small* **2015**, *11*, 3973–3984.
- (36) Wong, M. H.; Giraldo, J. P.; Kwak, S.-Y.; Koman, V. B.; Sinclair, R.; Lew, T. T. S.; Bisker, G.; Liu, P.; Strano, M. S. Nitroaromatic Detection and Infrared Communication from Wild-Type Plants Using Plant Nanobionics. *Nat. Mater.* **2017**, *16*, 264–272.
- (37) Koman, V. B.; Lew, T. T. S.; Wong, M. H.; Kwak, S.-Y.; Giraldo, J. P.; Strano, M. S. Persistent Drought Monitoring Using a Microfluidic-Printed Electro-Mechanical Sensor of Stomata in Planta. *Lab Chip*, **2017**, *17* 4015–4024.
- (38) Kwak, S.-Y.; Lew, T. T. S.; Sweeney, C. J.; Koman, V. B.; Wong, M. H.; Bohmert-Tatarev, K.; Snell, K. D.; Seo, J. S.; Chua, N.-H.; Strano, M. S. Chloroplast-Selective Gene Delivery and Expression in Planta Using Chitosan-Complexed Single-Walled Carbon Nanotube Carriers. *Nat. Nanotechnol.* **2019**, *14*, 447–455.
- (39) Demirer, G. S.; Zhang, H.; Matos, J. L.; Goh, N. S.; Cunningham, F. J.; Sung, Y.; Chang, R.; Aditham, A. J.; Chio, L.; Cho, M.-J.; Staskawicz, B.; Landry, M. P. High Aspect Ratio Nanomaterials Enable Delivery of Functional Genetic Material without DNA Integration in Mature Plants. *Nat. Nanotechnol.* **2019**, *14*, 456–464.
- (40) Le, V. N.; Rui, Y.; Gui, X.; Li, X.; Liu, S.; Han, Y. Uptake, Transport, Distribution and Bio-Effects of SiO<sub>2</sub> Nanoparticles in Bt-Transgenic Cotton. *J. Nanobiotechnology* **2014**, *12*, 50.
- (41) Gogos, A.; Moll, J.; Klingenfuss, F.; van der Heijden, M.; Irin, F.; Green, M. J.; Zenobi, R.; Bucheli, T. D. Vertical Transport and Plant Uptake of Nanoparticles in a Soil Mesocosm Experiment. *J. Nanobiotechnology* **2016**, *14*, 40.
- (42) Elmer, W. H.; White, J. C. The Use of Metallic Oxide Nanoparticles to Enhance Growth of Tomatoes and Eggplants in Disease Infested Soil or Soilless Medium. *Environ. Sci.: Nano*, **2016**, *3*, 1072–1079.
- (43) Sharma, P.; Sharma, A.; Sharma, M.; Bhalla, N.; Estrela, P.; Jain, A.; Thakur, P.; Thakur, A. Nanomaterial Fungicides: *In Vitro* and *In Vivo* Antimycotic Activity of Cobalt and Nickel Nanoferrites on Phytopathogenic Fungi. *Global Challenges*. **2017**, *1*, 1770071.
- (44) Kim, J.-H.; Oh, Y.; Yoon, H.; Hwang, I.; Chang, Y.-S. Iron Nanoparticle-Induced Activation of Plasma Membrane H<sup>+</sup>-ATPase Promotes Stomatal Opening in *Arabidopsis thaliana*. *Environ. Sci. Technol.* **2015**, *49*, 1113–1119.
- (45) Wu, H.; Santana, I.; Dansie, J.; Giraldo, J. P. *In Vivo* Delivery of Nanoparticles into Plant Leaves. *Curr. Protoc. Chem. Biol.* **2017**, *9*, 269–284.
- (46) Brillault, L.; Jutras, P. V.; Dashti, N.; Thuenemann, E. C.; Morgan, G.; Lomonossoff, G. P.;

- Landsberg, M. J.; Sainsbury, F. Engineering Recombinant Virus-Like Nanoparticles from Plants for Cellular Delivery. *ACS Nano* **2017**, *11*, 3476–3484.
- (47) Makhotenko, A. V.; Snigir, E. A.; Kalinina, N. O.; Makarov, V. V.; Taliansky, M. E. Data on a Delivery of Biomolecules into *Nicotiana benthamiana* Leaves Using Different Nanoparticles. *Data Brief* **2018**, *16*, 1034–1037.
- (48) Huang, X.; Stein, B. D.; Cheng, H.; Malyutin, A.; Tsvetkova, I. B.; Baxter, D. V.; Remmes, N. B.; Verchot, J.; Kao, C.; Bronstein, L. M.; Dragnea, B. Magnetic Virus-Like Nanoparticles in *N. benthamiana* Plants: A New Paradigm for Environmental and Agronomic Biotechnological Research. *ACS Nano* **2011**, *5*, 4037–4045.
- (49) Lv, J.; Christie, P.; Zhang, S. Uptake, Translocation, and Transformation of Metal-Based Nanoparticles in Plants: Recent Advances and Methodological Challenges. *Environ. Sci.: Nano* **2019**, *6*, 41–59.
- (50) Raliya, R.; Franke, C.; Chavalmane, S.; Nair, R.; Reed, N.; Biswas, P. Quantitative Understanding of Nanoparticle Uptake in Watermelon Plants. *Front. Plant Sci.* **2016**, *7*, 1288.
- (51) Karny, A.; Zinger, A.; Kajal, A.; Shainsky-Roitman, J.; Schroeder, A. Therapeutic Nanoparticles Penetrate Leaves and Deliver Nutrients to Agricultural Crops. *Sci. Rep.* **2018**, *8*, 7589.
- (52) Wang, W.-N.; Tarafdar, J. C.; Biswas, P. Nanoparticle Synthesis and Delivery by an Aerosol Route for Watermelon Plant Foliar Uptake. *J. Nanopart. Res.* **2013**, *15*, 1417.
- (53) Kranjc, E.; Mazej, D.; Regvar, M.; Drobne, D.; Remškar, M. Foliar Surface Free Energy Affects Platinum Nanoparticle Adhesion, Uptake, and Translocation from Leaves to Roots in Arugula and Escarole. *Environ. Sci.: Nano* **2018**, *5*, 520–532.
- (54) Etxeberría, E.; Gonzalez, P.; Bhattacharya, P.; Sharma, P.; Ke, P. C. Determining the Size Exclusion for Nanoparticles in Citrus Leaves. *HortScience* **2016**, *51*, 732–737.
- (55) Zhao, L.; Ortiz, C.; Adeleye, A. S.; Hu, Q.; Zhou, H.; Huang, Y.; Keller, A. A. Metabolomics to Detect Response of Lettuce (*Lactuca sativa*) to Cu(OH)<sub>2</sub> Nanopesticides: Oxidative Stress Response and Detoxification Mechanisms. *Environ. Sci. Technol.* **2016**, *50*, 9697–9707.
- (56) Hong, J.; Peralta-Videa, J. R.; Rico, C.; Sahi, S.; Viveros, M. N.; Bartonjo, J.; Zhao, L.; Gardea-Torresdey, J. L. Evidence of Translocation and Physiological Impacts of Foliar Applied CeO<sub>2</sub> Nanoparticles on Cucumber (*Cucumis sativus*) Plants. *Environ. Sci. Technol.* **2014**, *48*, 4376–4385.
- (57) Keller, A. A.; Huang, Y.; Nelson, J. Detection of Nanoparticles in Edible Plant Tissues Exposed to Nano-Copper Using Single-Particle ICP-MS. *J. Nanopart. Res.* **2018**, *20*, 101.
- (58) Larue, C.; Castillo-Michel, H.; Sobanska, S.; Cécillon, L.; Bureau, S.; Barthès, V.; Ouerdane, L.; Carrière, M.; Sarret, G. Foliar Exposure of the Crop *Lactuca sativa* to Silver Nanoparticles: Evidence for Internalization and Changes in Ag Speciation. *J. Hazard. Mater.* **2014**, *264*, 98–106.
- (59) Corredor, E.; Testillano, P. S.; Coronado, M.-J.; González-Melendi, P.; Fernández-Pacheco, R.; Marquina, C.; Ibarra, M. R.; de la Fuente, J. M.; Rubiales, D.; Pérez-de-Luque, A.; Risueño, M.-C. Nanoparticle Penetration and Transport in Living Pumpkin Plants: *In Situ* Subcellular Identification. *BMC Plant Biol.* **2009**, *9*, 45.
- (60) Li, H.; Huang, J.; Lu, F.; Liu, Y.; Song, Y.; Sun, Y.; Zhong, J.; Huang, H.; Wang, Y.; Li, S.; Lifshitz, Y.; Lee, S.-T.; Kang, Z. Impacts of Carbon Dots on Rice Plants: Boosting the Growth and Improving the Disease Resistance. *ACS Appl. Bio Mater.* **2018**, *1*, 663–672.
- (61) Ma, C.; White, J. C.; Zhao, J.; Zhao, Q.; Xing, B. Uptake of Engineered Nanoparticles by Food Crops: Characterization, Mechanisms, and Implications. *Annu. Rev. Food Sci. Technol.* **2018**, *9*, 129–153.
- (62) Rodrigues, S. M.; Trindade, T.; Duarte, A. C.; Pereira, E.; Koopmans, G. F.; Römkens, P. F. A. M. A Framework to Measure the Availability of Engineered Nanoparticles in Soils: Trends in Soil Tests and Analytical Tools. *Trends Analyt. Chem.* **2016**, *75*, 129–140.
- (63) Spielman-Sun, E.; Lombi, E.; Donner, E.; Howard, D.; Unrine, J. M.; Lowry, G. V. Impact of Surface Charge on Cerium Oxide Nanoparticle Uptake and Translocation by Wheat (*Triticum aestivum*). *Environ. Sci. Technol.* **2017**, *51*, 7361–7368.
- (64) Li, J.; Tappero, R. V.; Acerbo, A. S.; Yan, H.; Chu, Y.; Lowry, G. V.; Unrine, J. M. Effect of CeO<sub>2</sub>

- Nanomaterial Surface Functional Groups on Tissue and Subcellular Distribution of Ce in Tomato (*Solanum lycopersicum*). *Environ. Sci.: Nano* **2019**, *6*, 273–285.
- (65) Avellan, A.; Schwab, F.; Masion, A.; Chaurand, P.; Borschneck, D.; Vidal, V.; Rose, J.; Santaella, C.; Levard, C. Nanoparticle Uptake in Plants: Gold Nanomaterial Localized in Roots of *Arabidopsis thaliana* by X-Ray Computed Nanotomography and Hyperspectral Imaging. *Environ. Sci. Technol.* **2017**, *51*, 8682–8691.
- (66) Lew, T. T. S.; Wong, M. H.; Kwak, S.-Y.; Sinclair, R.; Koman, V. B.; Strano, M. S. Rational Design Principles for the Transport and Subcellular Distribution of Nanomaterials into Plant Protoplasts. *Small* **2018**, *14*, 1802086.
- (67) Schönherr, J. Characterization of Aqueous Pores in Plant Cuticles and Permeation of Ionic Solutes. *J. Exp. Bot.* **2006**, *57*, 2471–2491.
- (68) Kerstiens, G. Water Transport in Plant Cuticles: An Update. *J. Exp. Bot.* **2006**, *57*, 2493–2499.
- (69) Eichert, T.; Goldbach, H. E. Equivalent Pore Radii of Hydrophilic Foliar Uptake Routes in Stomatous and Astomatous Leaf Surfaces – Further Evidence for a Stomatal Pathway. *Physiol. Plant.* **2008**, *132*, 491–502.
- (70) Popp, C.; Burghardt, M.; Friedmann, A.; Riederer, M. Characterization of Hydrophilic and Lipophilic Pathways of *Hedera Helix* L. Cuticular Membranes: Permeation of Water and Uncharged Organic Compounds. *J. Exp. Bot.* **2005**, *56*, 2797–2806.
- (71) Eichert, T.; Kurtz, A.; Steiner, U.; Goldbach, H. E. Size Exclusion Limits and Lateral Heterogeneity of the Stomatal Foliar Uptake Pathway for Aqueous Solutes and Water-Suspended Nanoparticles. *Physiol. Plant.* **2008**, *134*, 151–160.
- (72) Zeng, Y.; Himmel, M. E.; Ding, S.-Y. Visualizing Chemical Functionality in Plant Cell Walls. *Biotechnol. Biofuels* **2017**, *10*, 263.
- (73) Albersheim, P.; Darvill, A.; Roberts, K.; Sederoff, R.; Staehelin, A. *Plant Cell Walls: From Chemistry to Biology*; Garland Science: New York, 2010; pp 241–242.
- (74) Starrach, N.; Mayer, W.-E. Unequal Distribution of Fixed Negative Charges in Isolated Cell Walls of Various Tissues in Primary Leaves of *Phaseolus*. *J. Plant Physiol.* **1986**, *126*, 213–222.
- (75) Fritz, E. Measurement of Cation Exchange Capacity (CEC) of Plant Cell Walls by X-Ray Microanalysis (EDX) in the Transmission Electron Microscope. *Microsc. Microanal.* **2007**, *13*, 233–244.
- (76) Meychik, N. R.; Yermakov, I. P. Ion Exchange Properties of Plant Root Cell Walls. *Plant Soil* **2001**, *234*, 181–193.
- (77) Szatanik-Kloc, A.; Szerement, J.; Józefaciuk, G. The Role of Cell Walls and Pectins in Cation Exchange and Surface Area of Plant Roots. *J. Plant Physiol.* **2017**, *215*, 85–90.
- (78) Li, X.; Rui, M.; Song, J.; Shen, Z.; Zeng, H. Carbon and Graphene Quantum Dots for Optoelectronic and Energy Devices: A Review. *Adv. Funct. Mater.* **2015**, *25*, 4929–4947.
- (79) Lim, S. Y.; Shen, W.; Gao, Z. Carbon Quantum Dots and Their Applications. *Chem. Soc. Rev.* **2015**, *44*, 362–381.
- (80) Wang, R.; Lu, K.-Q.; Tang, Z.-R.; Xu, Y.-J. Recent Progress in Carbon Quantum Dots: Synthesis, Properties and Applications in Photocatalysis. *J. Mater. Chem. A Mater. Energy Sustain.* **2017**, *5*, 3717–3734.
- (81) Das, R.; Bandyopadhyay, R.; Pramanik, P. Carbon Quantum Dots from Natural Resource: A Review. *Mater. Today Chem.* **2018**, *8*, 96–109.
- (82) Yang, S.-T.; Cao, L.; Luo, P. G.; Lu, F.; Wang, X.; Wang, H.; Mezziani, M. J.; Liu, Y.; Qi, G.; Sun, Y.-P. Carbon Dots for Optical Imaging *In Vivo*. *J. Am. Chem. Soc.* **2009**, *131*, 11308–11309.
- (83) Cao, L.; Mezziani, M. J.; Sahu, S.; Sun, Y.-P. Photoluminescence Properties of Graphene *versus* Other Carbon Nanomaterials. *Acc. Chem. Res.* **2013**, *46*, 171–180.
- (84) Song, Y.; Zhu, S.; Yang, B. Bioimaging Based on Fluorescent Carbon Dots. *RSC Adv.* **2014**, *4*, 27184–27200.
- (85) Zheng, Y.; Xie, G.; Zhang, X.; Chen, Z.; Cai, Y.; Yu, W.; Liu, H.; Shan, J.; Li, R.; Liu, Y.; Lei, B. Bioimaging Application and Growth-Promoting Behavior of Carbon Dots from Pollen on



- Hydroponically Cultivated Rome Lettuce. *ACS Omega* **2017**, *2*, 3958–3965.
- (86) Qian, K.; Guo, H.; Chen, G.; Ma, C.; Xing, B. Distribution of Different Surface Modified Carbon Dots in Pumpkin Seedlings. *Sci. Rep.* **2018**, *8*, 7991.
- (87) Torney, F.; Trewyn, B. G.; Lin, V. S.-Y.; Wang, K. Mesoporous Silica Nanoparticles Deliver DNA and Chemicals into Plants. *Nat. Nanotechnol.* **2007**, *2*, 295–300.
- (88) Chang, F.-P.; Kuang, L.-Y.; Huang, C.-A.; Jane, W.-N.; Hung, Y.; Hsing, Y.-I. C.; Mou, C.-Y. A Simple Plant Gene Delivery System Using Mesoporous Silica Nanoparticles as Carriers. *J. Mater. Chem. B Mater. Biol. Med.* **2013**, *1*, 5279–5287.
- (89) Martin-Ortigosa, S.; Peterson, D. J.; Valenstein, J. S.; Lin, V. S.-Y.; Trewyn, B. G.; Lyznik, L. A.; Wang, K. Mesoporous Silica Nanoparticle-Mediated Intracellular Cre Protein Delivery for Maize Genome Editing *via* loxP Site Excision. *Plant Physiol.* **2014**, *164*, 537–547.
- (90) Rastogi, A.; Tripathi, D. K.; Yadav, S.; Chauhan, D. K.; Živčák, M.; Ghorbanpour, M.; El-Sheery, N. I.; Brestic, M. Application of Silicon Nanoparticles in Agriculture. *3 Biotech* **2019**, *9*, 90.
- (91) Lin, B.-S.; Diao, S.-Q.; Li, C.-H.; Fang, L.-J.; Qiao, S.-C.; Yu, M. Effect of TMS (Nanostructured Silicon Dioxide) on Growth of Changbai Larch Seedlings. *Res. J. For.* **2004**, *15*, 138–140.
- (92) Siddiqui, M. H.; Al-Wahaibi, M. H. Role of Nano-SiO<sub>2</sub> in Germination of Tomato (*Lycopersicon esculentum* Seeds Mill.). *Saudi J. Biol. Sci.* **2014**, *21*, 13–17.
- (93) Spielman-Sun, E.; Avellan, A.; Bland, G. D.; Tappero, R. V.; Acerbo, A. S.; Unrine, J. M.; Giraldo, J. P.; Lowry, G. V. Nanoparticle Surface Charge Influences Translocation and Leaf Distribution in Vascular Plants with Contrasting Anatomy. *Environ. Sci.: Nano* **2019**, *6*, 2508–2519.
- (94) Raven, P. H.; Eichhorn, S. E.; Evert, R. F. *Biology of Plants*, 7th ed.; W.H. Freeman and Company: New York, 2005.
- (95) Benedict, C. R.; McCree, K. J.; Kohel, R. J. High Photosynthetic Rate of a Chlorophyll Mutant of Cotton. *Plant Physiol.* **1972**, *49*, 968–971.
- (96) Maroco, J. P.; Edwards, G. E.; Ku, M. S. Photosynthetic Acclimation of Maize to Growth under Elevated Levels of Carbon Dioxide. *Planta* **1999**, *210*, 115–125.
- (97) Buick, R. D.; Buchan, G. D.; Field, R. J. The Role of Surface Tension of Spreading Droplets in Absorption of a Herbicide Formulation *via* Leaf Stomata. *Pestic. Sci.* **1993**, *38*, 227–235.
- (98) Field, R. J.; Bishop, N. G. Promotion of Stomatal Infiltration of Glyphosate by an Organosilicone Surfactant Reduces the Critical Rainfall Period. *Pestic. Sci.* **1988**, *24*, 55–62.
- (99) Stevens, P. J. G. Organosilicone Surfactants as Adjuvants for Agrochemicals. *Pestic. Sci.* **1993**, *38*, 103–122.
- (100) Castro, M. J. L.; Ojeda, C.; Cirelli, A. F. Surfactants in Agriculture. In *Green Materials for Energy, Products and Depollution*; Lichtfouse, E., Schwarzbauer, J., Robert, D., Eds; Springer Netherlands: Dordrecht, 2013; pp 287–334.
- (101) Knoche, M. Organosilicone Surfactant Performance in Agricultural Spray Application: A Review. *Weed Res.* **1994**, *34*, 221–239.
- (102) Castro, M. J. L.; Ojeda, C.; Cirelli, A. F. Advances in Surfactants for Agrochemicals. *Environ. Chem. Lett.* **2014**, *12*, 85–95.
- (103) Avellan, A.; Yun, J.; Zhang, Y.; Spielman-Sun, E.; Unrine, J. M.; Thieme, J.; Li, J.; Lombi, E.; Bland, G.; Lowry, G. V. Nanoparticle Size and Coating Chemistry Control Foliar Uptake Pathways, Translocation, and Leaf-To-Rhizosphere Transport in Wheat. *ACS Nano* **2019**, *13*, 5291–5305
- (104) Bao, W.; Wang, J.; Wang, Q.; O'Hare, D.; Wan, Y. Layered Double Hydroxide Nanotransporter for Molecule Delivery to Intact Plant Cells. *Sci. Rep.* **2016**, *6*, 26738.
- (105) Zeiger, E. The Biology of Stomatal Guard Cells. *Annu. Rev. Plant Physiol.* **1983**, *34*, 441–474.
- (106) Araújo, W. L.; Fernie, A. R.; Nunes-Nesi, A. Control of Stomatal Aperture: A Renaissance of the Old Guard. *Plant Signal. Behav.* **2011**, *6*, 1305–1311.
- (107) McLachlan, D. H.; Kopischke, M.; Robatzek, S. Gate Control: Guard Cell Regulation by Microbial Stress. *New Phytol.* **2014**, *203*, 1049–1063.
- (108) Geilfus, C.-M. The pH of the Apoplast: Dynamic Factor with Functional Impact Under Stress. *Mol. Plant* **2017**, *10*, 1371–1386.

- 1  
2  
3 (109) Wu, H.; Shabala, L.; Liu, X.; Azzarello, E.; Zhou, M.; Pandolfi, C.; Chen, Z.-H.; Bose, J.;  
4 Mancuso, S.; Shabala, S. Linking Salinity Stress Tolerance with Tissue-Specific Na<sup>+</sup> Sequestration  
5 in Wheat Roots. *Front. Plant Sci.* **2015**, *6*, 71.
- 6 (110) Dunn, K. W.; Kamocka, M. M.; McDonald, J. H. A Practical Guide to Evaluating Colocalization  
7 in Biological Microscopy. *Am. J. Physiol. Cell Physiol.* **2011**, *300*, C723–C742.
- 8 (111) Williams, W. E.; Gorton, H. L.; Witiak, S. M. Chloroplast Movements in the Field. *Plant Cell*  
9 *Environ.* **2003**, *26*, 2005–2014.
- 10 (112) Trojan, A.; Gabrys, H. Chloroplast Distribution in *Arabidopsis thaliana* (L.) Depends on Light  
11 Conditions during Growth. *Plant Physiol.* **1996**, *111*, 419–425.
- 12 (113) Wada, M. Chloroplast Movement. *Plant Sci.* **2013**, *210*, 177–182.
- 13 (114) Lin, J.; Alexander-Katz, A. Cell Membranes Open “Doors” for Cationic  
14 Nanoparticles/Biomolecules: Insights into Uptake Kinetics. *ACS Nano* **2013**, *7*, 10799–10808.
- 15 (115) Chen, J.; Hessler, J. A.; Putchakayala, K.; Panama, B. K.; Khan, D. P.; Hong, S.; Mullen, D. G.;  
16 Dimaggio, S. C.; Som, A.; Tew, G. N.; Lopatin, A. N.; Baker, J. R.; Holl, M. M. B.; Orr, B. G.  
17 Cationic Nanoparticles Induce Nanoscale Disruption in Living Cell Plasma Membranes. *J. Phys.*  
18 *Chem. B* **2009**, *113*, 11179–11185.
- 19 (116) Rui, Y.; Chen, Y.; Kandemir, B.; Yi, H.; Wang, J. Z.; Puri, V. M.; Anderson, C. T. Balancing  
20 Strength and Flexibility: How the Synthesis, Organization, and Modification of Guard Cell Walls  
21 Govern Stomatal Development and Dynamics. *Front. Plant Sci.* **2018**, *9*, 1202.
- 22 (117) Freudling, C.; Starrach, N.; Flach, D.; Gradmann, D.; Mayer, W. E. Cell Walls as Reservoirs of  
23 Potassium Ions for Reversible Volume Changes of Pulvinar Motor Cells during Rhythmic Leaf  
24 Movements. *Planta* **1988**, *175*, 193–203.
- 25 (118) Wolterbeek, H. T. Cation Exchange in Isolated Xylem Cell Walls of Tomato. I. Cd<sup>2+</sup> and Rb<sup>+</sup>  
26 Exchange in Adsorption Experiments. *Plant Cell Environ.* **1987**, *10*, 39–44.
- 27 (119) Lundqvist, M.; Stigler, J.; Elia, G.; Lynch, I.; Cedervall, T.; Dawson, K. A. Nanoparticle Size and  
28 Surface Properties Determine the Protein Corona with Possible Implications for Biological Impacts.  
29 *Proc. Natl. Acad. Sci. U. S. A.* **2008**, *105*, 14265–14270.
- 30 (120) Monopoli, M. P.; Walczyk, D.; Campbell, A.; Elia, G.; Lynch, I.; Bombelli, F. B.; Dawson, K. A.  
31 Physical-Chemical Aspects of Protein Corona: Relevance to *In Vitro* and *In Vivo* Biological Impacts  
32 of Nanoparticles. *J. Am. Chem. Soc.* **2011**, *133*, 2525–2534.
- 33 (121) Durán, N.; Silveira, C. P.; Durán, M.; Martínez, D. S. T. Silver Nanoparticle Protein Corona and  
34 Toxicity: A Mini-Review. *J. Nanobiotechnology* **2015**, *13*, 55.
- 35 (122) Barbir, R.; Goessler, W.; Čurlin, M.; Micek, V.; Milić, M.; Vuković, B.; Milić, M.; Ljubojević,  
36 M.; Domazet Jurašin, D.; Vinković Vrček, I. Protein Corona Modulates Distribution and  
37 Toxicological Effects of Silver Nanoparticles *In Vivo*. *Part. Part. Syst. Charact.* **2019**, *18*, 1900174.
- 38 (123) Pitek, A. S.; Wen, A. M.; Shukla, S.; Steinmetz, N. F. The Protein Corona of Plant Virus  
39 Nanoparticles Influences Their Dispersion Properties, Cellular Interactions, and *In Vivo* Fates. *Small*  
40 **2016**, *12*, 1758–1769.
- 41 (124) Ponnuel, S.; Subramanian, B.; Ponnuraj, K. Conformational Change Results in Loss of  
42 Enzymatic Activity of Jack Bean Urease on Its Interaction with Silver Nanoparticle. *Protein J.* **2015**,  
43 *34*, 329–337.
- 44 (125) Yamaoka, K.; Nakagawa, T.; Uno, T. Statistical Moments in Pharmacokinetics. *J.*  
45 *Pharmacokinet. Biopharm.* **1978**, *6*, 547–558.
- 46 (126) Shargel, L.; Wu-Pong, S.; Yu, A. *Applied Biopharmaceutics & Pharmacokinetics, Fifth Edition*;  
47 McGraw Hill Professional: New York, 2004; pp 1–30.
- 48 (127) Gibaldi, M. *Compartmental and Noncompartmental Pharmacokinetics, Fourth edition*; Lea &  
49 Feiber Philadelphia: Malvern, PA, 1991; pp 1–13.
- 50 (128) Andes, D.; Craig, W. A. Animal Model Pharmacokinetics and Pharmacodynamics: A Critical  
51 Review. *Int. J. Antimicrob. Agents* **2002**, *19*, 261–268.
- 52 (129) Graham, M. A.; Lockwood, G. F.; Greenslade, D.; Brienza, S.; Bayssas, M.; Gamelin, E. Clinical  
53 Pharmacokinetics of Oxaliplatin: A Critical Review. *Clin. Cancer Res.* **2000**, *6*, 1205–1218.
- 54  
55  
56  
57  
58  
59  
60

- 1  
2  
3 (130) Glass, P. S. A.; Gan, T. J.; Howell, S. A Review of the Pharmacokinetics and Pharmacodynamics  
4 of Remifentanyl. *Anesthesia & Analgesia* **1999**, *89*, 7–14.
- 5 (131) Khan, W. U.; Wang, D.; Zhang, W.; Tang, Z.; Ma, X.; Ding, X.; Du, S.; Wang, Y. High Quantum  
6 Yield Green-Emitting Carbon Dots for Fe(III) Detection, Biocompatible Fluorescent Ink and  
7 Cellular Imaging. *Sci. Rep.* **2017**, *7*, 14866.
- 8 (132) Asati, A.; Santra, S.; Kaittanis, C.; Nath, S.; Perez, J. M. Oxidase-like Activity of Polymer-  
9 Coated Cerium Oxide Nanoparticles. *Angew. Chem. Int. Ed Engl.* **2009**, *48*, 2308–2312.
- 10 (133) Collin, B.; Oostveen, E.; Tsyusko, O. V.; Unrine, J. M. Influence of Natural Organic Matter and  
11 Surface Charge on the Toxicity and Bioaccumulation of Functionalized Ceria Nanoparticles in  
12 *Caenorhabditis elegans*. *Environ. Sci. Technol.* **2014**, *48*, 1280–1289.
- 13 (134) Asati, A.; Santra, S.; Kaittanis, C.; Perez, J. M. Surface-Charge-Dependent Cell Localization and  
14 Cytotoxicity of Cerium Oxide Nanoparticles. *ACS Nano* **2010**, *4*, 5321–5331.
- 15 (135) Larson, D. R.; Ow, H.; Vishwasrao, H. D.; Heikal, A. A.; Wiesner, U.; Webb, W. W. Silica  
16 Nanoparticle Architecture Determines Radiative Properties of Encapsulated Fluorophores. *Chem.*  
17 *Mater.* **2008**, *20*, 2677–2684.
- 18 (136) Lowry, G. V.; Hill, R. J.; Harper, S.; Rawle, A. F. Guidance to Improve the Scientific Value of  
19 Zeta-Potential Measurements in nanoEHS. *Environmentalist* **2016**, *3*, 953–965.
- 20 (137) Doane, T. L.; Chuang, C.-H.; Hill, R. J.; Burda, C. Nanoparticle  $\zeta$ -Potentials. *Acc. Chem. Res.*  
21 **2012**, *45*, 317–326.
- 22 (138) Skoglund, S.; Hedberg, J.; Yunda, E.; Godymchuk, A.; Blomberg, E.; Odnevall Wallinder, I.  
23 Difficulties and Flaws in Performing Accurate Determinations of Zeta Potentials of Metal  
24 Nanoparticles in Complex Solutions-Four Case Studies. *PLoS One* **2017**,  
25 DOI.10.1371/journal.pone.0181735
- 26 (139) Pradhan Mitra, P.; Loqué, D. Histochemical Staining of *Arabidopsis thaliana* Secondary Cell  
27 Wall Elements. *J. Vis. Exp.* **2014**, DOI.org/10.3791/51381.
- 28 (140) Jelínková, A.; Malínská, K.; Simon, S.; Kleine-Vehn, J.; Parezová, M.; Pejchar, P.; Kubes, M.;  
29 Martinec, J.; Friml, J.; Zazimalová, E.; Petrásek, J. Probing Plant Membranes with FM Dyes:  
30 Tracking, Dragging or Blocking? *Plant J.* **2010**, *61*, 883–892.
- 31 (141) Emans, N.; Zimmermann, S.; Fischer, R. Uptake of a Fluorescent Marker in Plant Cells Is  
32 Sensitive to Brefeldin A and Wortmannin. *Plant Cell* **2002**, *14*, 71–86.
- 33 (142) Bolte, S.; Talbot, C.; Boutte, Y.; Catrice, O.; Read, N. D.; Satiat-Jeunemaitre, B. FM-Dyes as  
34 Experimental Probes for Dissecting Vesicle Trafficking in Living Plant Cells. *J. Microsc.* **2004**, *214*,  
35 159–173.
- 36 (143) Mullineaux, D. R. CI2 for Creating and Comparing Confidence-Intervals for Time-Series  
37 Bivariate Plots. *Gait Posture* **2017**, *52*, 367–373.
- 38 (144) Zaiontz, C. Confidence Ellipse Analysis Tool, 2019. Real Statistics Using Excel.  
39 [https://www.real-statistics.com/multivariate-statistics/multivariate-normal-distribution/confidence-](https://www.real-statistics.com/multivariate-statistics/multivariate-normal-distribution/confidence-ellipse-analysis-tool/)  
40 [ellipse-analysis-tool/](https://www.real-statistics.com/multivariate-statistics/multivariate-normal-distribution/confidence-ellipse-analysis-tool/) (accessed March 8, 2020)
- 41  
42  
43  
44  
45  
46  
47  
48  
49  
50  
51  
52  
53  
54  
55  
56  
57  
58  
59  
60

# Table of Content

1  
2  
3  
4  
5  
6  
7  
8  
9  
10  
11  
12  
13  
14  
15  
16  
17  
18  
19  
20  
21  
22  
23  
24  
25  
26  
27  
28  
29  
30  
31  
32  
33  
34  
35  
36  
37  
38  
39  
40  
41  
42  
43  
44  
45  
46  
47  
48  
49  
50  
51  
52  
53  
54  
55  
56  
57  
58  
59  
60

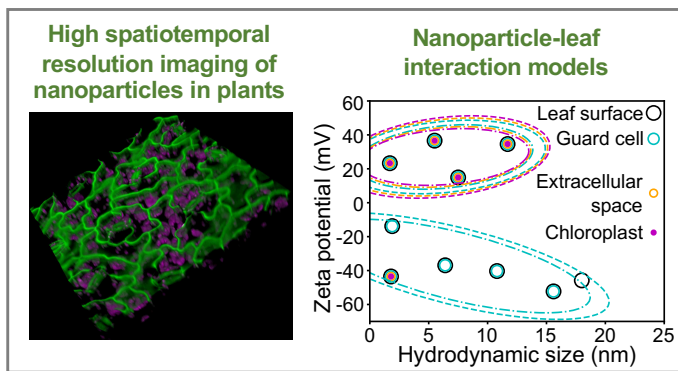
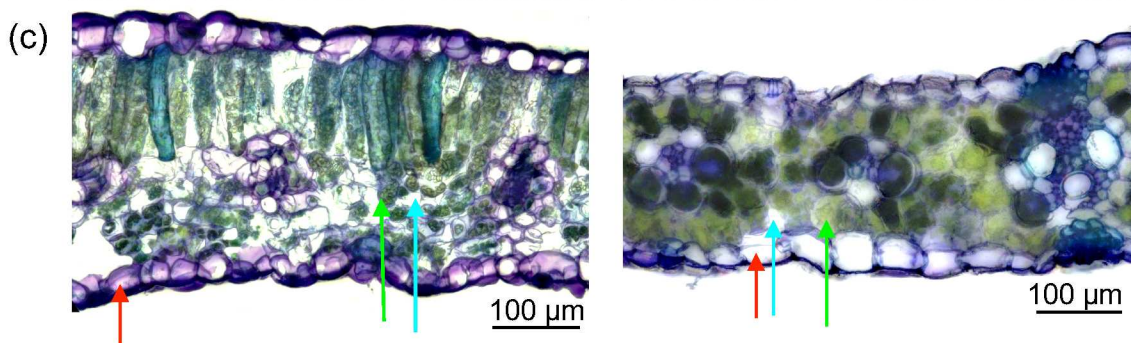
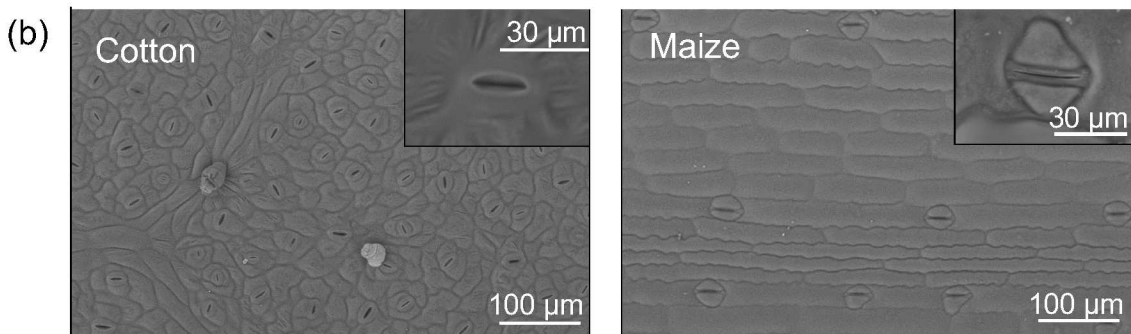
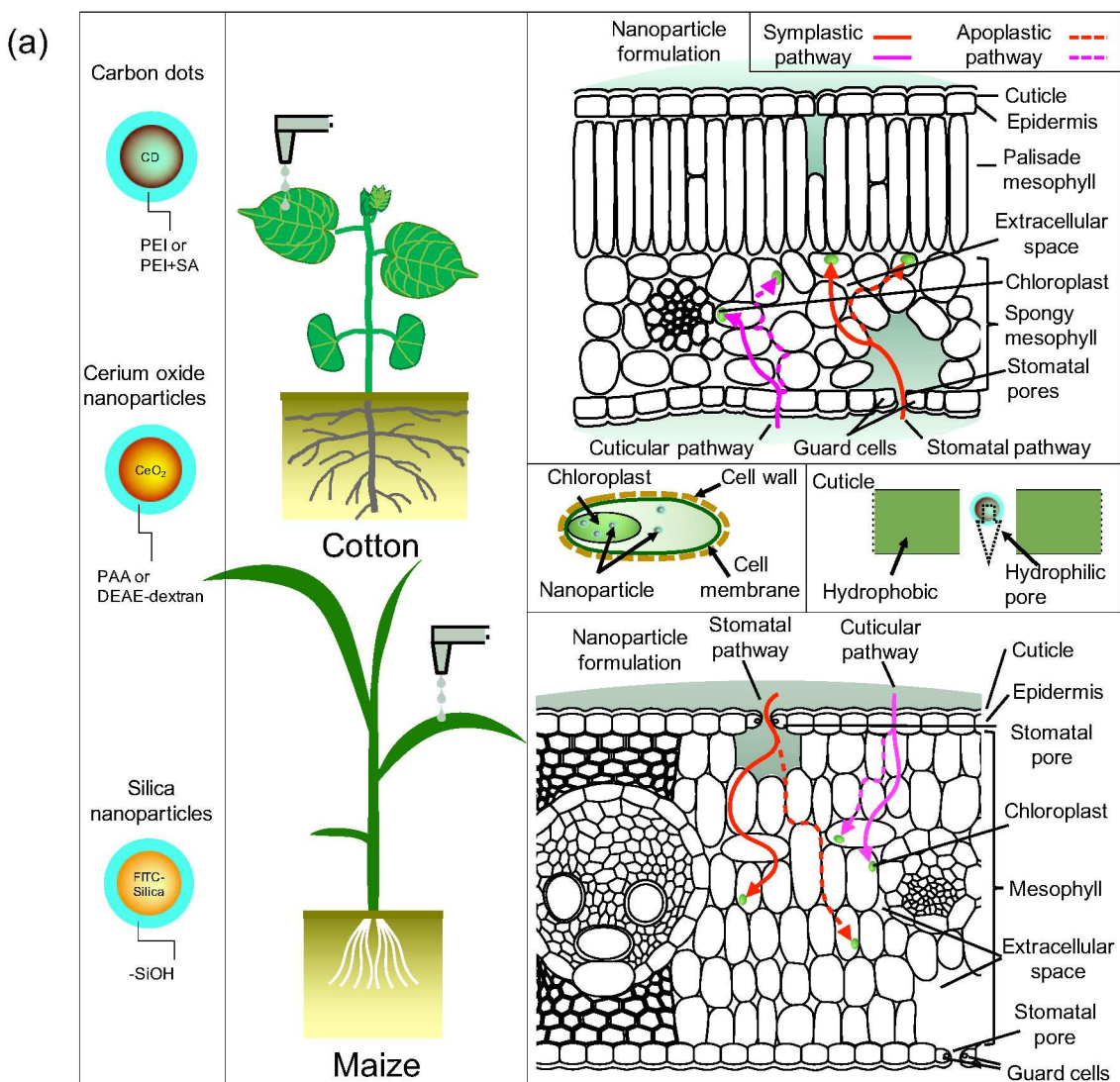


Figure 1



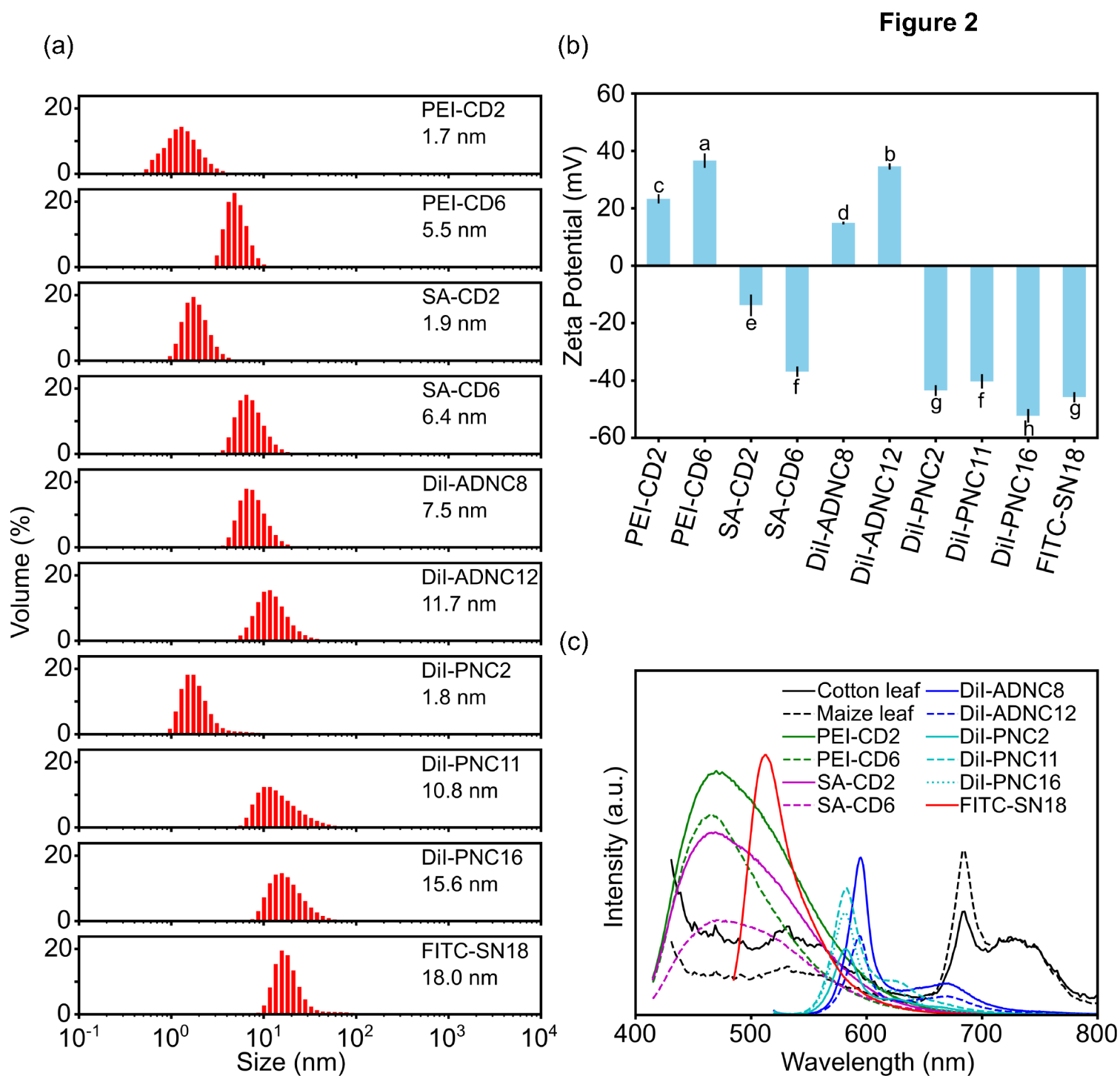


Figure 3

(a)

	Cotton				Maize			
	PEI-CD2	SA-CD2	PEI-CD6	SA-CD6	PEI-CD2	SA-CD2	PEI-CD6	SA-CD6
Triton X-100	No leaf NP uptake	No leaf NP uptake	No leaf NP uptake	No leaf NP uptake	Leaf NP uptake	Leaf NP uptake	No leaf NP uptake	No leaf NP uptake
Silwet L-77	Leaf NP uptake	Leaf NP uptake	Leaf NP uptake	Leaf NP uptake	Leaf NP uptake	Leaf NP uptake	Leaf NP uptake	Leaf NP uptake

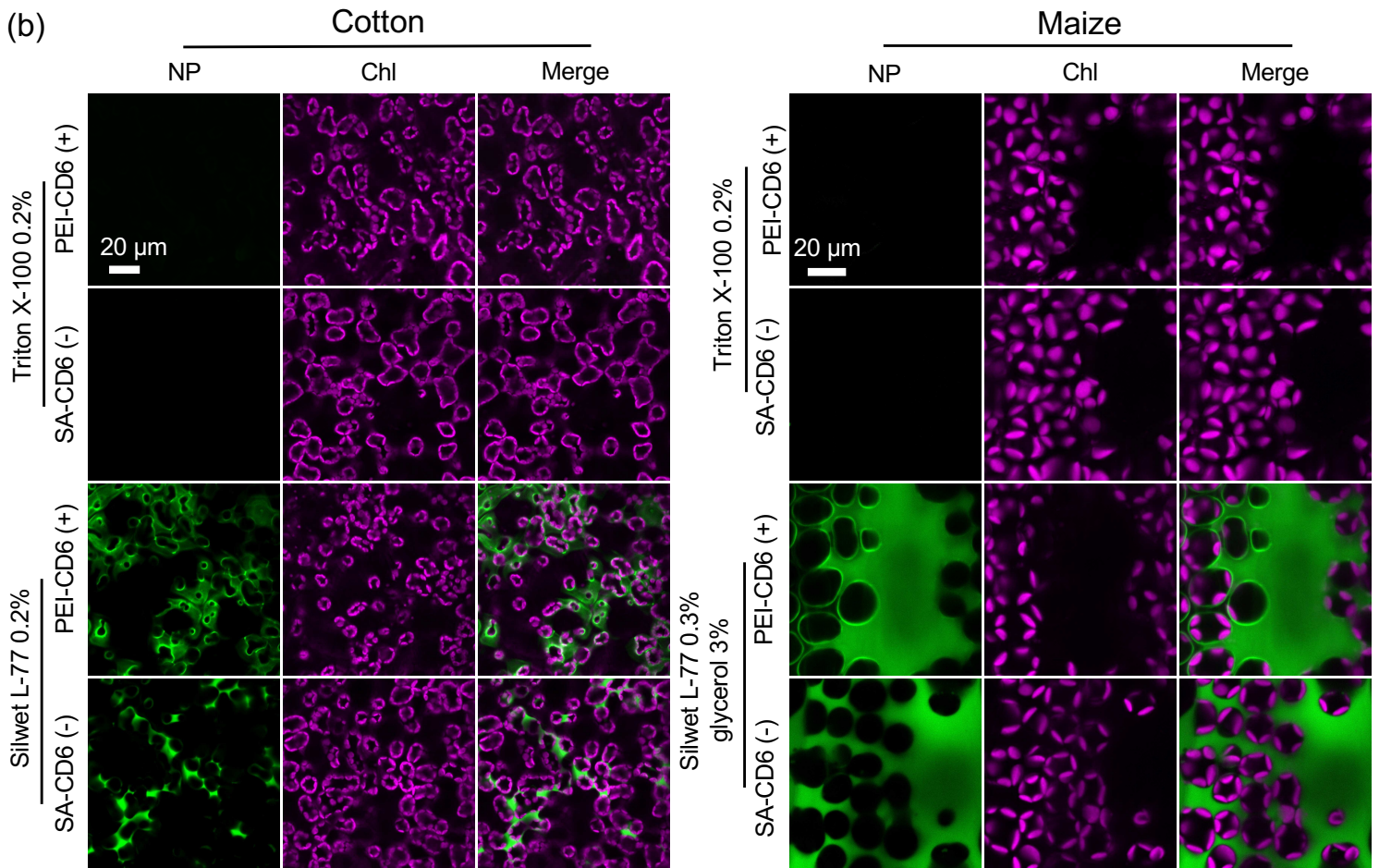


Figure 4

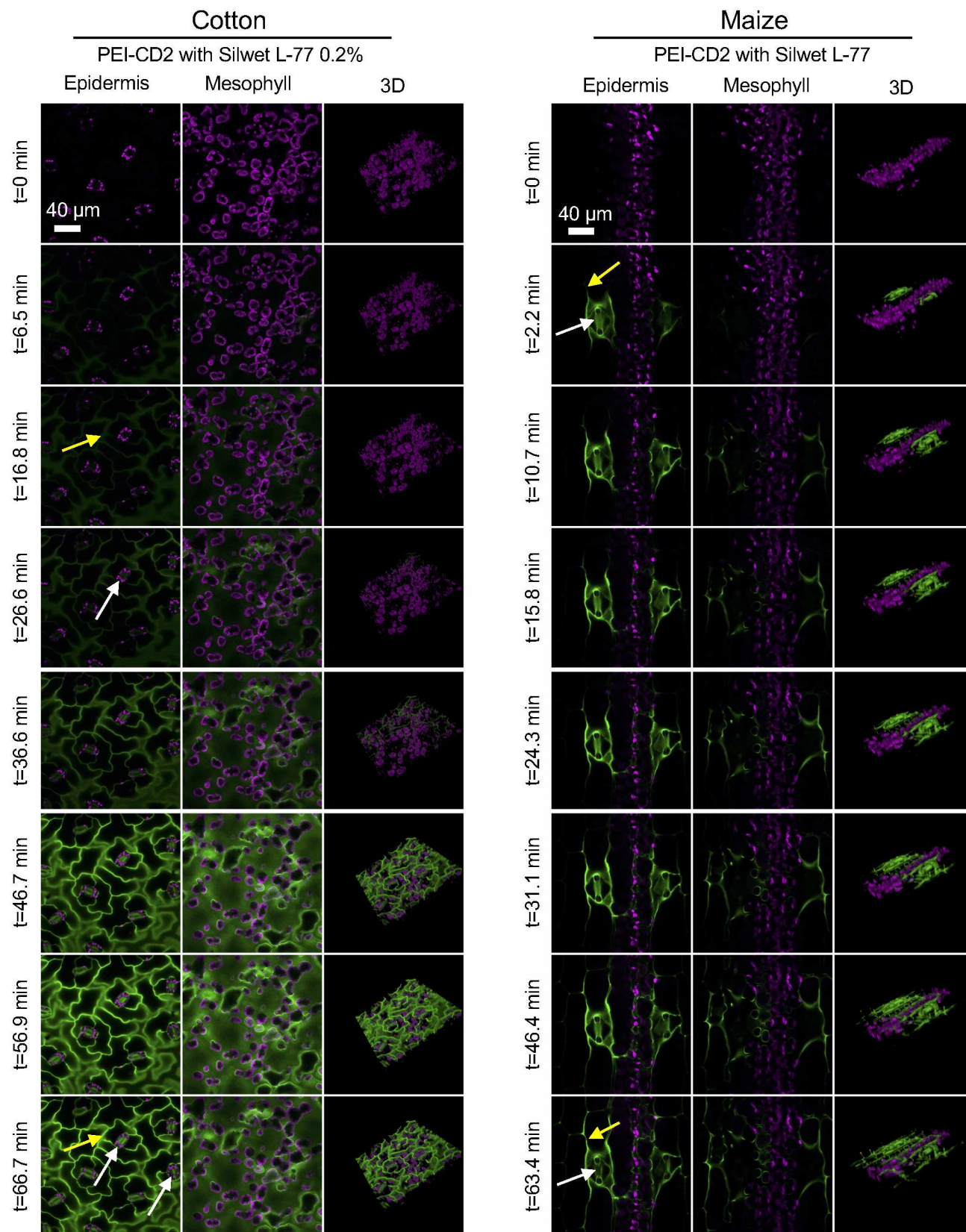




Figure 5

